BRCA1 was the first breast cancer susceptibility gene to be identified (in 1990).[27] The majority of this gene was cloned in 1994 by Miki and colleagues.[28] Previous studies indicate that higher *BRCA1* methylation levels in breast cancer correlate with more advanced tumor stages at diagnosis and are associated with a 45% increase in mortality compared with patients who have unmethylated *BRCA1* promoters.[29] In our patients, the frequency of *BRCA1* methylation in resected stage II or III NSCLC was 14.6% (data not shown), compared with 18.6% in stage I patients. These data indicate there is no apparent relationship between *BRCA1* methylation level and tumor stage in lung cancer. We demonstrated that methylation of the *BRCA1* promoter gene correlates with lower recurrence-free survival in patients with curatively resected pathological stage I NSCLC; however, *BRCA1* promoter methylation status was not associated with any clinicopathological features, including pathological stage. Interestingly, 5 patients showed *BRCA1* methylation in tumor tissue and adjacent normal lung tissue as well. Three of these 5 patients developed recurrent tumor; however, the characteristics of recurrence status seem to be nonspecific. Although it is not clear whether these 5 patients possessed germline methylation of *BRCA1*, positive unmethylation status was demonstrated in noncancerous tissue, and the degree of methylation in noncancerous tissue was not strong compared with cancerous tissue. Furthermore, epigenetic alteration initiated by exposure to carcinogens in tobacco smoke is one of the main causes of lung cancer, and tobacco smoking plays a significant role in the prognosis of patients with lung cancer.[30] Despite these facts, no association between *BRCA1* promoter methylation and smoking status was observed in this study.

Several molecular markers have been identified for use as both prognostic tools and targets for novel therapeutic approaches. Such molecular markers also help to identify patients who would benefit from specific anticancer therapies. A growing body of evidence indicates that BRCA1 plays a central role in DNA repair and in cell cycle control.[31,32] A lack of functional BRCA1 leads to increased sensitivity of tumor cells to molecular damage, suggesting that BRCA1 could be used as a predictive molecular marker to identify patients who would benefit from specific anticancer therapies. According to the results of several investigations, BRCA1 confers sensitivity to apoptosis induced by antimicrotubule drugs (eg, paclitaxel and vincristine), but induces resistance to DNA-damaging agents (eg, cisplatin and etoposide) and radiotherapy.[33–36] Because adjuvant chemotherapy is currently a matter of great debate, particularly regarding its use in curatively resected NSCLC, *BRCA1* methylation could be a promising molecular marker for predicting not only the disease outcome but also the effectiveness of chemotherapy. In this study, the small sample size limited the assessment of differences in the effects of chemotherapy between patients with methylated *BRCA1* and those without. Further investigations using a larger sample size are needed to determine whether assessment of *BRCA1* methylation status provides clinical information relevant to tailored adjuvant therapy.

In summary, we observed methylation of the *BRCA1* promoter in 13 of 70 (18.6%) cases of curatively resected stage I NSCLC and determined that such methylation was an independent risk factor for tumor recurrence. *BRCA1* methylation status was not associated with any specific clinicopathological features, including pathological stage. These results indicate that *BRCA1* methylation plays an important role in the progression of NSCLC and that *BRCA1* methylation is a promising biomarker that predicts the outcome of disease after curative resection of stage I NSCLC. *BRCA1* has been recognized as a promising genetic determinant of responses to different types of chemotherapy; therefore, further studies using larger samples are warranted to investigate the usefulness of determining a patient's *BRCA1* methylation status. Such studies should be designed with a special emphasis on establishing customized adjuvant treatment strategies for patients with curatively resected stage I NSCLC.

FUNDING SOURCES

This work was supported, in part, by Grants-in-Aid for the Third-term Comprehensive 10-Year Strategy for Cancer Control from the Ministry of Health, Labour and Welfare of Japan; Grants-in-Aid for Cancer Research from the Ministry of Education, Culture, Science, Sports, and Technology of Japan; Research Funding from Kyowa Hakko; and Research Funding from Daiwa Securities Health Foundation.

CONFLICT OF INTEREST DISCLOSURE

The authors made no disclosure.

REFERENCES

1. Dominioni L, Imperatori A, Rovera F, et al. Stage I nonsmall cell lung carcinoma: analysis of survival and implications for screening. *Cancer* 2000;89(11 suppl):2334–2344.
2. Goodgame B, Stinchcombe TE, Simon G, Wozniak A, Govindan R. Recent advances in lung cancer: summary of presentations from the 45th annual meeting of the American Society of Clinical Oncology (2009). *J Thorac Oncol.* 2009;4:1293–1300.

3. Brock MV, Hooker CM, Ota-Machida E, et al. DNA methylation markers and early recurrence in stage I lung cancer. *N Engl J Med.* 2008;358:1118–1128.
4. Ushijima T. Detection and interpretation of altered methylation patterns in cancer cells. *Nat Rev Cancer.* 2005;5:223–231.
5. Jones PA, Baylin SB. The fundamental role of epigenetic events in cancer. *Nat Rev Genet.* 2002;3:415–428.
6. Baylin SB, Herman JG, Graff JR, Vertino PM, Issa JP. Alterations in DNA methylation: a fundamental aspect of neoplasia. *Adv Cancer Res.* 1998;72:141–196.
7. Herman JG, Baylin SB. Gene silencing in cancer in association with promoter hypermethylation. *N Engl J Med.* 2003;349:2042–2054.
8. Kim JS, Kim JW, Han J, Shim YM, Park J, Kim DH. Cohypermethylation of p16 and FHIT promoters as a prognostic factor of recurrence in surgically resected stage I non-small cell lung cancer. *Cancer Res.* 2006;66:4049–4054.
9. Merlo A, Herman JG, Mao L, et al. 5′ CpG island methylation is associated with transcriptional silencing of the tumour suppressor p16/CDKN2/MTS1 in human cancers. *Nat Med.* 1995;1:686–692.
10. Dammann R, Li C, Yoon JH, Chin PL, Bates S, Pfeifer GP. Epigenetic inactivation of a RAS association domain family protein from the lung tumour suppressor locus 3p21.3. *Nat Genet.* 2000; 25:315–319.
11. Gu J, Berman D, Lu C, et al. Aberrant promoter methylation profile and association with survival in patients with non-small cell lung cancer. *Clin Cancer Res.* 2006;12:7329–7338.
12. Ford D, Easton DF, Stratton M, et al. Genetic heterogeneity and penetrance analysis of the BRCA1 and BRCA2 genes in breast cancer families. The Breast Cancer Linkage Consortium. *Am J Hum Genet.* 1998;62:676–689.
13. Dobrovic A, Simpfendorfer D. Methylation of the BRCA1 gene in sporadic breast cancer. *Cancer Res.* 1997;57:3347–3350.
14. Esteller M, Silva JM, Dominguez G, et al. Promoter hypermethylation and BRCA1 inactivation in sporadic breast and ovarian tumors. *J Natl Cancer Inst.* 2000;92:564–569.
15. Campan M, Weisenberger DJ, Laird PW. DNA methylation profiles of female steroid hormone-driven human malignancies. *Curr Top Microbiol Immunol.* 2006;310:141–178.
16. Thompson D, Easton DF. Cancer Incidence in BRCA1 mutation carriers. *J Natl Cancer Inst.* 2002;94:1358–1365.
17. Taron M, Rosell R, Felip E, et al. BRCA1 mRNA expression levels as an indicator of chemoresistance in lung cancer. *Hum Mol Genet.* 2004;13:2443–2449.
18. Marsit CJ, Liu M, Nelson HH, Posner M, Suzuki M, Kelsey KT. Inactivation of the Fanconi anemia/BRCA pathway in lung and oral cancers: implications for treatment and survival. *Oncogene.* 2004;23: 1000–1004.
19. Lee MN, Tseng RC, Hsu HS, et al. Epigenetic inactivation of the chromosomal stability control genes BRCA1, BRCA2, and XRCC5 in non-small cell lung cancer. *Clin Cancer Res.* 2007;13:832–838.
20. Kennedy RD, Quinn JE, Johnston PG, Harkin DP. BRCA1: mechanisms of inactivation and implications for management of patients. *Lancet.* 2002;360:1007–1014.
21. Miyamoto K, Asada K, Fukutomi T, et al. Methylation-associated silencing of heparan sulfate D-glucosaminyl 3-O-sulfotransferase-2 (3-OST-2) in human breast, colon, lung and pancreatic cancers. *Oncogene.* 2003;22:274–280.
22. Herman JG, Graff JR, Myöhänen S, Nelkin BD, Baylin SB. Methylation-specific PCR: a novel PCR assay for methylation status of CpG islands. *Proc Natl Acad Sci U S A.* 1996;93:9821–9826.
23. Miyamoto K, Fukutomi T, Akashi-Tanaka S, et al. Identification of 20 genes aberrantly methylated in human breast cancers. *Int J Cancer.* 2005;116:407–414.
24. Furuta J, Umebayashi Y, Miyamoto K, et al. Promoter methylation profiling of 30 genes in human malignant melanoma. *Cancer Sci.* 2004;95:962–968.
25. Wang Y, Zhang D, Zheng W, Luo J, Bai Y, Lu Z. Multiple gene methylation of nonsmall cell lung cancers evaluated with 3-dimensional microarray. *Cancer.* 2008;112:1325–1336.
26. Miyamoto K, Fukutomi T, Asada K, et al. Promoter hypermethylation and post-transcriptional mechanisms for reduced BRCA1 immunoreactivity in sporadic human breast cancers. *Jpn J Clin Oncol.* 2002;32:79–84.
27. Hall JM, Lee MK, Newman B, et al. Linkage of early-onset familial breast cancer to chromosome 17q21. *Science.* 1990;250: 1684–1689.
28. Miki Y, Swensen J, Shattuck-Eidens D, et al. A strong candidate for the breast and ovarian cancer susceptibility gene BRCA1. *Science.* 1994;266:66-71.
29. Xu X, Gammon MD, Zhang Y, et al. BRCA1 promoter methylation is associated with increased mortality among women with breast cancer. *Breast Cancer Res Treat.* 2009;115:397–404.
30. Rom WN, Hay JG, Lee TC, Jiang Y, Tchou-Wong KM. Molecular and genetic aspects of lung cancer. *Am J Respir Crit Care Med.* 2000;161(4 pt 1):1355–1367.
31. Reguart N, Cardona AF, Carrasco E, Gomez P, Taron M, Rosell R. BRCA1: a new genomic marker for non-small-cell lung cancer. *Clin Lung Cancer.* 2008;9:331–339.
32. Rosell R, Perez-Roca L, Sanchez JJ, et al. Customized treatment in non-small-cell lung cancer based on EGFR mutations and BRCA1 mRNA expression. *PLoS One.* 2009;4:e5133.
33. Lafarge S, Sylvain V, Ferrara M, Bignon YJ. Inhibition of BRCA1 leads to increased chemoresistance to microtubule-interfering agents, an effect that involves the JNK pathway. *Oncogene.* 2001;20:6597–6606.
34. Husain A, He G, Venkatraman ES, Spriggs DR. BRCA1 up-regulation is associated with repair-mediated resistance to cis-diamminedichloroplatinum(II). *Cancer Res.* 1998;58:1120–1123.
35. Bhattacharyya A, Ear US, Koller BH, Weichselbaum RR, Bishop DK. The breast cancer susceptibility gene BRCA1 is required for subnuclear assembly of Rad51 and survival following treatment with the DNA cross-linking agent cisplatin. *J Biol Chem.* 2000;275: 23899–23903.
36. Abbott DW, Thompson ME, Robinson-Benion C, Tomlinson G, Jensen RA, Holt JT. BRCA1 expression restores radiation resistance in BRCA1-defective cancer cells through enhancement of transcription-coupled DNA repair. *J Biol Chem.* 1999;274:18808–18812.

International Journal of
Radiation Oncology
biology • physics

www.redjournal.org

Biology Contribution

Influence of Age on the Relative Biological Effectiveness of Carbon Ion Radiation for Induction of Rat Mammary Carcinoma

Tatsuhiko Imaoka, PhD,* Mayumi Nishimura,* Kazuhiro Daino, PhD,* Toshiaki Kokubo, PhD, DVM,† Kazutaka Doi, PhD,‡ Daisuke Iizuka, PhD, DVM,*,§ Yukiko Nishimura,* Tomomi Okutani, MS,*,‖ Masaru Takabatake, MRS,*,¶ Shizuko Kakinuma, PhD,* and Yoshiya Shimada, PhD*

**Radiobiology for Children's Health Program, Research Center for Radiation Protection, and †Department of Technical Support and Development, Research Development and Support Center, and ‡Regulatory Sciences Research Program, Research Center for Radiation Protection, National Institute of Radiological Sciences, Chiba, Japan; §Department of Molecular Radiobiology, Research Institute for Radiation Biology and Medicine, Hiroshima University, Hiroshima, Japan; ‖Department of Biology, Graduate School of Science, Chiba University, Chiba, Japan; and ¶Department of Radiological Sciences, Graduate School of Human Health Sciences, Tokyo Metropolitan University, Tokyo, Japan*

Received Feb 10, 2012, and in revised form Aug 3, 2012. Accepted for publication Aug 14, 2012

Summary

The risk of secondary cancer in children after particle radiation therapy is unclear. Using rats, we show that the period spanning neonatal development and early adulthood, but not fetal development or full adulthood, is associated with susceptibility to mammary carcinogenesis after γ-ray exposure. The effectiveness of a 290-MeV/u carbonion

Purpose: The risk of developing secondary cancer after radiotherapy, especially after treatment of childhood cancers, remains a matter of concern. The high biological effects of carbon-ion radiation have enabled powerful radiotherapy, yet the approach is commonly restricted to the treatment of adults. Susceptibility of the fetus to particle radiation–induced cancer is also unclear. The present study is aimed to investigate the effect of carbon-ion irradiation in childhood on breast carcinogenesis.

Methods and Materials: We irradiated female Sprague-Dawley rats of various ages (embryonic days 3, 13, and 17 and 1, 3, 7, and 15 weeks after birth) with ^{137}Cs γ rays or a 290-MeV/u monoenergetic carbonion beam (linear energy transfer, 13 keV/μm). All animals were screened weekly for mammary carcinoma by palpation until they were 90 weeks old.

Results: Irradiation of fetal and mature (15-week-old) rats with either radiation source at a dose of 0.2 or 1 Gy did not substantially increase the hazard ratio compared with the nonirradiated group. Dose responses (0.2-2.0 Gy) to γ rays were similar among the groups of rats irradiated 1, 3, and 7 weeks after birth. The effect of carbon ions increased along with the age at the time of irradiation, indicating relative biological effectiveness values of 0.2 (−0.3, 0.7), 1.3 (1.0, 1.6), and 2.8 (1.8, 3.9) (mean and 95% confidence interval) for animals that were 1, 3, and 7 weeks of age, respectively.

Reprint requests to: Tatsuhiko Imaoka, PhD, 4-9-1 Anagawa, Inage-ku, Chiba 263-8555, Japan. Tel: (+81) 43-206-4053; Fax: (+81) 43-206-4138; E-mail: t_imaoka@nirs.go.jp

This work was supported in part by a Grant-In-Aid for Young Scientists (B) from the Ministry of Education, Culture, Sports, Science and Technology of Japan (grant 23710074) and is a part of the Research Projects with Heavy Ions at NIRS-HIMAC (projects 17B239 and 20B239).

Conflicts of interest: none.

Supplementary material for this article can be found at www.redjournal.org.

Acknowledgment—The authors thank Dr Takashi Takabatake (deceased) for his contribution to the work; Drs. Akihiro Nakata, Kazumi Yamauchi, Kentaro Ariyoshi, Yi Shang and the staff at the Research, Development and Support Center, National Institute of Radiological Sciences, for technical assistance.

Int J Radiation Oncol Biol Phys, Vol. 85, No. 4, pp. 1134–1140, 2013
0360-3016/$ - see front matter
http://dx.doi.org/10.1016/j.ijrobp.2012.08.035

beam (13 keV/μm) in inducing mammary cancer is also age dependent, with the greatest effectiveness seen in early adulthood and the least effectiveness seen for neonates.

Conclusions: Our findings imply that carbonion therapy may be associated with a risk of secondary breast cancer in humans, the extent of which may depend on the age of the patient at the time of irradiation.

Introduction

Particle radiation therapy continues to improve cancer treatment by permitting accurate dose localization and strong biological effects attributed to the sharp Bragg peak and high linear energy transfer (LET) (1). The National Institute of Radiological Sciences (NIRS) in Japan, where clinical studies using carbonion radiation from the Heavy-Ion Medical Accelerator in Chiba (HIMAC) have been conducted since 1994, is one of several facilities of its kind in the world (1). Because Bragg peaks are normally too narrow for therapeutic applications, spread-out Bragg peaks (SOBP) have been devised to obtain a broad and uniform dose distribution (2). Fractionated irradiation with a beam with 6-cm SOBP, which is developed from the 290-MeV/u carbon ions and has a LET range of 40 to 90 keV/μm within the SOBP component, has been used to treat several cancer types.

There is increasing concern that medical radiation exposure can increase the risk of cancer, especially in children. Breast tissue is susceptible to radiation-induced carcinogenesis, and epidemiologic studies have suggested a high risk of breast cancer after radiation exposure during childhood (3, 4). Carbonion radiation therapy is currently not applied for the treatment of childhood cancers, partly because of the potential risk of promoting secondary cancer. Previous studies have indicated the high relative biological effectiveness (RBE) of heavy ions, such as carbon ions, for the induction of cancer in mammary glands and other sites (5-8). We previously reported a high RBE for the induction of mammary carcinogenesis in rats irradiated with a 6-cm SOBP carbonion beam at 7 weeks after birth (ie, early adulthood) (5). Because the mammary gland is one of the organs irradiated during radiation therapy for tumors in the chest area, it is likely that healthy mammary tissue will be exposed to the relatively low-LET (13 keV/μm) component of the carbonion beam. Nevertheless, there is no published information from studies conducted in humans or using animal models about the risk of carcinogenesis after carbon-ion irradiation, whether fractionated or single, during childhood.

Apart from clinical issues, evidence suggests high susceptibility of the fetus to radiogenic cancer (9). Indeed, neutrons are reported to impose high cancer risk to fetal mice (10), indicating a need for basic knowledge on the consequence of fetal exposure to heavy ions. In the present study we used a common rat model of mammary carcinogenesis to investigate the effects of irradiation with 13 keV/μm carbon ions on rats of various ages in comparison with rats irradiated with γ rays.

Methods and Materials

Heavy-ion and γ-ray irradiation

Carbon-ion irradiation was conducted at the HIMAC in NIRS; the 290-MeV/u monoenergetic carbonion beam (LET, 13 keV/μm in the plateau region; diameter, 11 cm) was used. Each rat was placed in a cylinder-shaped, 1-cm-thick polymethylmethacrylate chamber 10 cm deep and with a diameter of 10 cm, which was set in the plateau region of the beam. The absorbed dose of carbon ions was calculated as described previously (2). The duration of irradiation ranged from 1 to 2 minutes, resulting in an average dose rate of 0.1 to 3.0 Gy/min. The γ-irradiation was performed as previously described (5) using a ^{137}Cs γ-irradiator at a dose rate of 0.6 Gy/min.

Animal experiments

All animal experiments were approved by the Institutional Animal Care and Use Committee of NIRS. Female Sprague-Dawley rats (Jcl:SD; Clea Japan, Tokyo, Japan) were housed in autoclaved cages and maintained in rooms with controlled temperature (23°C ± 1°C) and humidity (50% ± 5%) under a regular 12-hour light/12-hour dark cycle with a standard laboratory diet (CE-2; Clea Japan) and water provided ad libitum. Pregnant rats (postcoitus days 3, 13, and 17) and postnatal rats (weeks 1, 3, 7, and 15 after birth) were either whole-body irradiated with γ rays or carbon ions at 0.2, 0.5, 1.0, or 2.0 Gy or left unirradiated under pentobarbital-mediated anesthesia (30-35 mg/kg, for reduction of stress during transportation between the breeding and irradiation facilities), as outlined in the experimental plan shown in Table 1. The number of animals per group was 21 to 43, as indicated in

Table 1 Experimental groups

Symbol	Age at irradiation	Stage of development	Dose irradiated (Gy)
0 Gy	Not irradiated	Unirradiated control	0
E3	Embryonic day 3	Fetal, pre-implantation	0.2
E13	Embryonic day 13	Fetal, major organogenesis	0.2, 1.0
E17	Embryonic day 17	Fetal, late stage	0.2, 1.0
1W	1 wk after birth	Neonatal	0.2, 0.5, 1.0, 2.0
3W	3 wk after birth	Prepubertal	0.2, 0.5, 1.0, 2.0
7W	7 wk after birth	Early adulthood	0.2, 0.5, 1.0, 2.0
15W	15 wk after birth	Full adulthood	0.2, 1.0

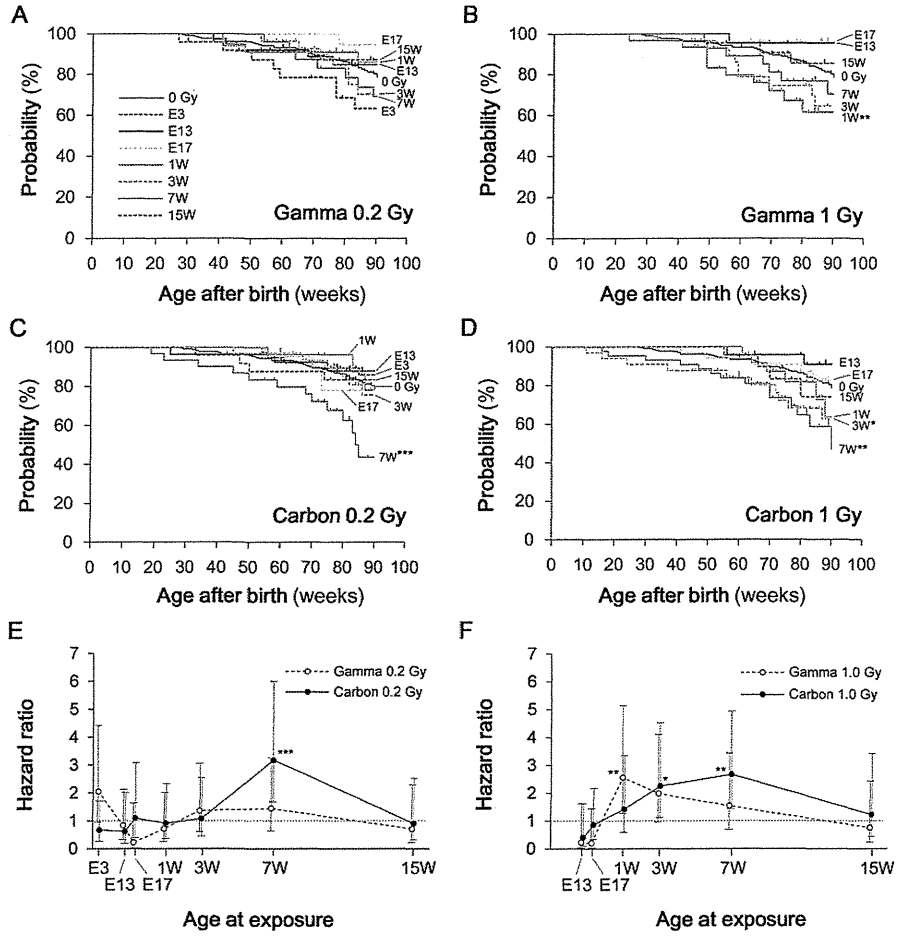

Fig. 1. Mammary carcinogenesis after irradiation with γ rays and carbon ions at various ages between embryonic and adulthood stages. (A-D) Kaplan-Meier plots for carcinoma-free survival of rats left unirradiated (0 Gy; common in A-D) and irradiated with γ rays (Gamma) or carbon ions (Carbon) at embryonic day 3, 13, or 17 (E3, E13, and E17, respectively) or 1, 3, 7, or 15 weeks after birth (1W, 3W, 7W, and 15W, respectively). (E, F) Cox proportional hazard ratio plotted against the age at irradiation. Vertical bars indicate the 95% confidence interval. $*P<.05$; $**P<.01$; $***P<.001$ versus 0 Gy by the log-rank test.

Table e1 (available online; www.redjournal.org). Rats not exposed to γ- or carbon-ion irradiation together constituted the control group (217 rats). After maternal irradiation, 6 to 7 pups were raised by a dam. Juvenile rats were weaned at day 21 after birth. During weekly observations, any tumor that was detected by palpation was recorded. Estrous cycles were recorded monthly for 5 consecutive days according to the cytology of vaginal smears ($n=3$ for each irradiated group; $n=9$ for the control group). Rats were killed if they showed any signs of general deterioration over the course of the experiment. The experiment was terminated when rats that had survived to an age of 90 weeks were killed by exsanguination under ether anesthesia and then autopsied. Excised tumors were fixed in 10% neutral-buffered formalin, and 2-μm-thick paraffin-embedded sections were prepared and stained with hematoxylin and eosin for histologic evaluation (11). For the palpable carcinoma-free survival analysis, the first appearance of a palpable carcinoma was estimated retrospectively from both pathology results at autopsy and the tumor palpation history.

Statistics

Cox proportional hazard analysis was performed for the palpable carcinoma-free survival time (ie, time to the first palpation of carcinoma) using the free statistical software R (http://www.r-project.org/). Animal death before the first detection of carcinoma by palpation was classified as censoring. A χ^2 test was performed for comparison of the tumor incidence; Yates' correction was used for analysis where frequency values were <5. Dunnett's test was used to assess differences from the control group with respect to the age at the time of cessation of the regular estrous cycle. The measure for statistical significance was $P<.05$. The relationship between the dose (in Grays) and hazard ratio was fitted to a linear equation with a y-intercept of 1 by the least-square method. Excess relative risk (ERR) (Gy^{-1}) was defined as the estimated slope of the line. Given that RBE is generally defined as the ratio of doses of 2 radiation species that give an identical biological effect, we defined it as the ratio of ERR values obtained for each of the 2 types of radiation. Standard errors of the ratio values were calculated using the delta method.

Results

Female Sprague-Dawley rats at various stages of development (embryonic days 3, 13, and 17 and 1, 3, 7, and 15 weeks after birth) were irradiated with ^{137}Cs γ rays or 290 MeV/u

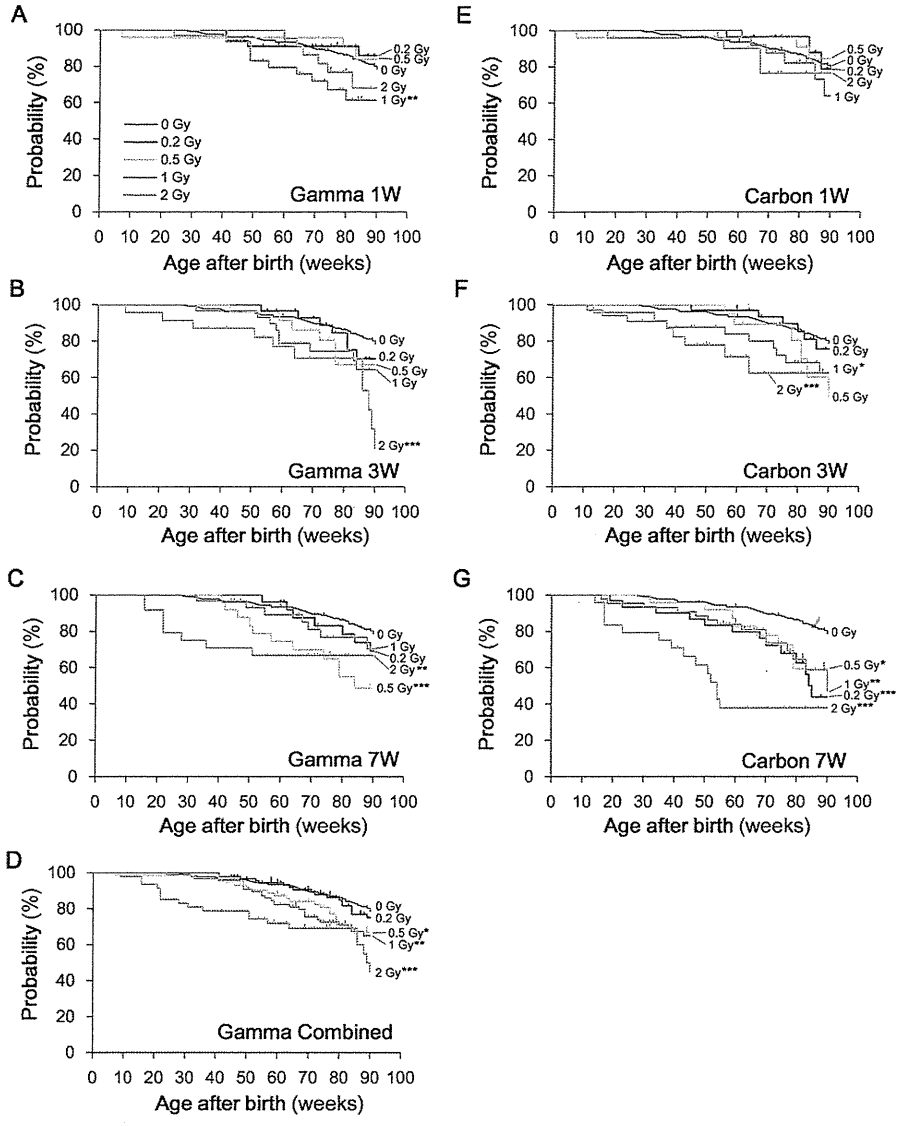

Fig. 2. Kaplan-Meier plots for mammary carcinoma-free survival in rats irradiated with various doses of γ rays or carbon ions at 1, 3, or 7 weeks of age. (A-C) Rats were left unirradiated (0 Gy; common in all panels) or irradiated with 0.2, 0.5, 1.0, or 2.0 Gy of γ rays (Gamma) at 1, 3, or 7 weeks after birth (1W, 3W, and 7W, respectively). (D) Data in A-C were pooled and reanalyzed, except for the group irradiated with 2.0 Gy at 1 week after birth, in which precocious cessation of the estrous cycle occurred. (E-G) Rats were irradiated with carbon ions (Carbon) as in A-C. $*P<.05$; $**P<.01$; $***P<.001$ versus 0 Gy by the log-rank test.

monoenergetic carbon ions (with an LET of 13 keV/μm) at the doses indicated in Table 1. A group of nonirradiated rats was subjected to the same analysis to enable comparison. All rats were observed weekly for development of palpable mammary tumors until 90 weeks of age (or earlier if general deterioration of an animal required that it be killed), after which the animals were killed. Excised mammary tumors were analyzed histologically and classified as either adenocarcinoma or benign tumors, such as adenoma and fibroadenoma. Although carcinoma constituted a minor fraction of the tumors, its raw incidence at autopsy ranged from 7% to 71% among groups, indicating that carcinoma development was indeed increased in some of the irradiated groups compared with the unirradiated control group (24%; Table e1). However, the observation period (ie, the age at the time of autopsy) also differed between groups (64-89 weeks; Table e1). The timing of autopsy was delayed in one group, and this was analyzed further (Table e2). In addition, the incidence of lung metastasis of mammary carcinoma did not show clear difference between the 2 radiation species (Table e1), in contrast to our previous observation of high incidence for the SOBP carbon ion beam (5). The results of delivery and development of pups after fetal irradiation are summarized in Table e3; we did not make a selection of pups on the basis of their defects.

To compare the susceptibility to carcinoma induction among the wide range of ages at irradiation, the palpable carcinoma-free survival time was analyzed using the Kaplan-Meier method for those groups in which rats were irradiated with γ rays or carbon ions at 0.2 Gy or 1.0 Gy (Fig. 1A-D). The hazard ratio for the development of palpable carcinoma was calculated according to these data using Cox proportional hazard model (Fig. 1E and F). As a result, γ irradiation at 1 week of age (1.0 Gy) and carbonion irradiation at 3 weeks (1.0 Gy) and 7 weeks (0.2 and 1.0 Gy) of

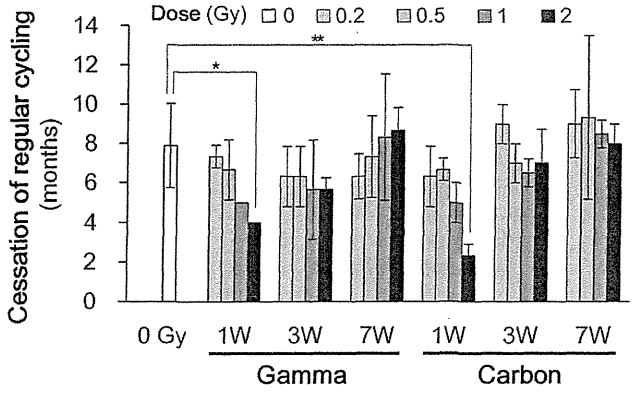

Fig. 3. Age at cessation of the regular estrous cycle. Female rats were irradiated with 0.2 to 2.0 Gy of γ rays (Gamma) or carbon ions (Carbon) at 1, 3, or 7 weeks after birth (1W, 3W, and 7W, respectively) or left unirradiated (0 Gy). For all treatments, the vaginal smear was scored monthly for 5 consecutive days. Bars indicate the mean age at the cessation of regular cycling, with the vertical bars indicating standard deviation. $*P<.05$; $**P<.01$ versus 0 Gy.

age significantly increased the risk of carcinogenesis. The comparison thus shows that, for rats, the period of susceptibility to radiation-induced mammary carcinogenesis lies between 1 and 7 weeks after birth, with minimal susceptibility after irradiation during either the embryonic or full-adulhood stage.

Dose-effect relationships were then analyzed for experiments involving irradiation with γ rays or carbon ions at 1, 3, and 7 weeks after birth. The palpable carcinoma-free survival data indicated an overall tendency of dose-dependent increases in carcinoma development (Fig. 2A-C and E-G). It seemed, however, that the highest dose (2.0 Gy) of radiation at 1 week of age caused no clear increase in rates of carcinogenesis (Fig. 2A and E). We reasoned that this latter effect might be attributed to the highly effective diminishment of the ovarian follicular pool that occurs after neonatal irradiation of rats (12). Indeed, γ or carbonion irradiation at 1 week of age (2.0 Gy) induced premature cessation of the estrous cycle (Fig. 3). Therefore, these 2 data points were excluded from the analysis of the dose-effect relationship (Fig. 4A and E, open circles). In this analysis, plotting of hazard ratios against dose indicated similar effects of γ irradiation among the groups of rats irradiated between 1 and 7 weeks after birth (Fig. 4A-C). In contrast, the effect of carbon ions was greater for animals irradiated at later stages of development (Fig. 4E-G).

To derive RBE values for carbonion irradiation at different ages, we first calculated the value of ERR (Gy^{-1}) for each combination of radiation and age, as defined by the increase in the hazard ratio with unit dose (Table 2). We tentatively used a linear fitting because the present data, composed of 5 dose groups, were not suitable for detailed analysis of the shape of the dose response, and because linear dose response has been frequently observed for radiation carcinogenesis (4-7). The ERR values of the γ-ray groups fell within close proximity, having mutually overlapping confidence intervals (Table 2). Therefore, we combined these γ-ray groups to form a new set of dose-effect relationship data (Figs. 2D and 4D) to obtain a better estimation of ERR for γ rays (Table 2, bottom row); because significant effects on the estrous cycle were observed, as mentioned above, after 2.0 Gy irradiation at 1 week of age, these data were excluded. The RBE values for carbonion irradiation were first calculated as the ratio of ERR for carbon ions to ERR of γ rays within each age group, giving the values 0.2, 1.1, and 3.3 for irradiation at 1, 3, and 7 weeks of age, respectively (Table 2, second-to-last column). The use of ERR for the combined γ-ray data as a reference resulted in similar values of 0.2, 1.3, and 2.8, respectively, with smaller confidence intervals (Table 2, rightmost column). Thus, the data suggested lower RBE values for breast cancer risk from carbonion irradiation of neonates and juveniles compared with that of young adults.

Discussion

The present study indicates that postnatal weeks 1 to 7 is the period during which rats are most susceptible to γ-ray induced mammary carcinogenesis. In contrast, irradiation with γ rays during the embryonic and full-adulthood stages does not significantly increase the risk of mammary carcinoma. These results agree with the epidemiologic observation that fetal exposure to the atomic bomb radiation (which mostly consisted of γ rays) is associated with a relatively low risk of solid cancer compared with the risk after exposure during early childhood (13). On the other hand, another study on the atomic bomb survivors indicated that a high excess absolute risk (EAR) of breast cancer is associated with exposure at an early age (4). ERR is, however, independent of the age at the time of exposure, because of the varying background incidence among the groups of different ages at exposure (4). The present observation of susceptibility during childhood and young adulthood but not at full adulthood (15 weeks of age in rat) resembles the EAR result, supporting the idea that EAR is more likely to reflect the biologically relevant period of susceptibility.

The present evidence suggests that induction of mammary carcinoma by carbonion irradiation is less likely in neonates and juveniles than in young adults. The mechanistic basis of this novel observation is difficult to explain. Most prepubertal mammary cells are quiescent in the absence of hormone-induced cell proliferation and, therefore, they may not be proficient in homologous recombination, which operates in the late S or G2 phase of the cell cycle and is required for repairing carbon ion-induced complex DNA damages (14-16). Alternatively, cell cycle delays induced by the particle radiation may affect the proliferation of stem-like cells, which is most active in the prepubertal mammary gland (17), and suppress expansion of initiated cells. We also noted an association between premature cessation of estrous cycling and low susceptibility to mammary carcinogenesis. This may be relevant to the clinical situation whereby a high ovarian dose induces premature menopause and reduces the radiation therapy-associated risk of secondary breast cancer (18), implying modification of cancer risk by dose localization. Ovarian estrogen may be required for secretion of prolactin into circulation or of growth factors in the cancer microenvironment, both of which are known promoting factor for breast cancer (19).

Unlike humans, Sprague-Dawley rats show very high prevalence of mammary carcinoma if monitored over their lifetime, a limitation of the Sprague-Dawley rat model. Nevertheless, use of carbon ions for thoracic tumors of children (eg, osteosarcomas and chordoma) would result in exposure of the mammary tissue to doses and LET commensurate with the experimental situation used here (approximately 1.5 Gy per fraction, approximately 13 keV/μm). Irradiation of other areas will result in exposure to very low radiation doses from scattered beams (20), which is not tested

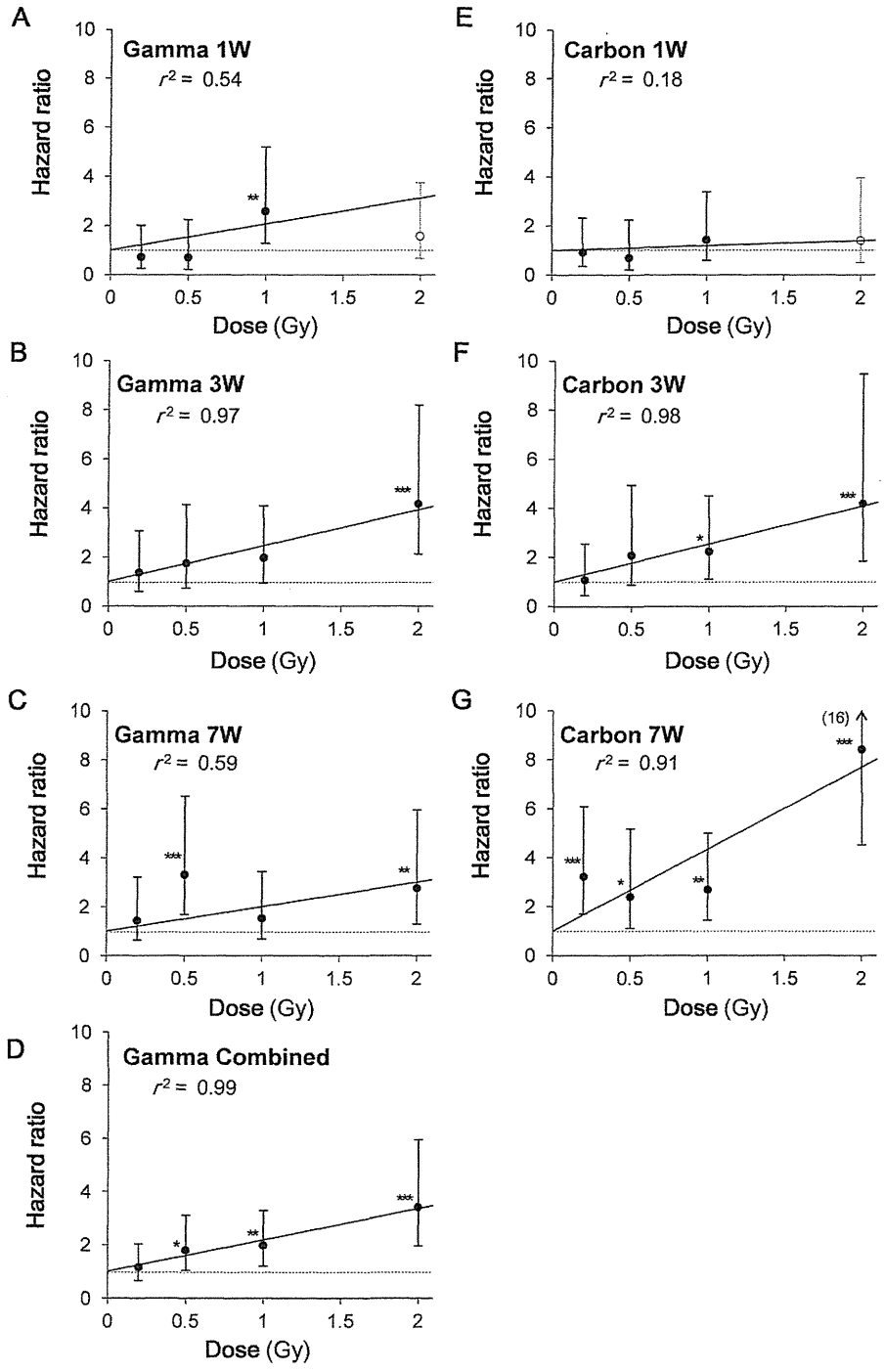

Fig. 4. Dose-effect relationship for induction of rat mammary carcinoma. Female rats were irradiated with 0.2-2.0 Gy of γ rays (A-D) or carbon ions (E-G) 1, 3, or 7 weeks after birth (1W, 3W, and 7W, respectively). The hazard ratio for the development of palpable mammary carcinoma is plotted against the dose. Vertical bars indicate the 95% confidence interval. Linear fitting was performed by the least-squares method, and the r^2 value is indicated in each panel. $^*P<.05$; $^{**}P<.01$; $^{***}P<.001$ versus 0 Gy by the log-rank test.

in these experiments. The absorbed dose from carbon ions to the normal tissue is generally less than one-third of that used in photon radiation therapies because of the high biological effect and improved dose localization (2); therefore, even for the highest RBE postulated in our study (ie, 2.8), the expected cancer risk would be lower than that anticipated for photon radiation therapies. Because exposure is localized and fractionated in clinical situations, future studies will be needed to clarify how such factors modify the carcinogenic effect. Investigations are also required regarding the effect on normal tissues at other sites, because the effect will likely depend on tissue type (4). Taken together, the present study provides evidence of a carcinogenic effect of carbon ions that depends on the age of the patient at the time of irradiation.

Table 2 Excess relative risk (ERR) per Gray of γ rays and 290 MeV/u monoenergetic carbon ions and relative biological effectiveness (RBE) of carbon ions for induction of rat mammary carcinoma

	ERR (Gy^{-1})*		RBE	
Age at exposure	γ rays	Carbon ions	Separate analysis†	Combined analysis‡
1 wk	1.1 (−0.3, 2.4)§	0.2 (−0.4, 0.8)	0.2 (−0.4, 0.8)	0.2 (−0.3, 0.7)
3 wk	1.5 (1.2, 1.7)	1.5 (1.3, 1.8)	1.1 (0.8, 1.3)	1.3 (1.0, 1.6)
7 wk	1.0 (0.1, 1.9)	3.3 (2.2, 4.5)	3.3 (0.0, 6.7)	2.8 (1.8, 3.9)
All ages combined‖	1.2 (1.0, 1.3)			

* Defined by least-squares fitting of hazard ratio data to 1 + ERR × dose (Gy) as in Figure 4.
† Calculated as the ratio of ERR of carbon ions to ERR of γ rays for each age.
‡ Calculated as the ratio of ERR of carbon ions for each age to ERR of γ rays for all ages combined.
§ Mean (95% confidence interval).
‖ Data for 1, 3, and 7 wk were combined and reanalyzed as in Figures 2D and 4D, except for the group irradiated with 2.0 Gy at 1 wk after birth, in which precocious cessation of the estrous cycle occurred.

References

1. Okada T, Kamada T, Tsuji H, et al. Carbon ion radiotherapy: Clinical experiences at National Institute of Radiological Science (NIRS). *J Radiat Res* 2010;51:355-364.
2. Kanai T, Endo M, Minohara S, et al. Biophysical characteristics of HIMAC clinical irradiation system for heavy-ion radiation therapy. *Int J Radiat Oncol Biol Phys* 1999;44:201-210.
3. Hancock SL, Tucker MA, Hoppe RT. Breast cancer after treatment of Hodgkin's disease. *J Natl Cancer Inst* 1993;85:25-31.
4. Preston DL, Ron E, Tokuoka S, et al. Solid cancer incidence in atomic bomb survivors: 1958-1998. *Radiat Res* 2007;168:1-64.
5. Imaoka T, Nishimura M, Kakinuma S, et al. High relative biologic effectiveness of carbon ion radiation on induction of rat mammary carcinoma and its lack of H-ras and Tp53 mutations. *Int J Radiat Oncol Biol Phys* 2007;69:194-203.
6. Dicello JF, Christian A, Cucinotta FA, et al. In vivo mammary tumourigenesis in the Sprague-Dawley rat and microdosimetric correlates. *Phys Med Biol* 2004;49:3817-3830.
7. Shellabarger CJ, Baum JW, Holtzman S, et al. Neon-20 ion- and X-ray-induced mammary carcinogenesis in female rats. *Ann N Y Acad Sci* 1985;459:239-244.
8. Durante M, Cucinotta FA. Heavy ion carcinogenesis and human space exploration. *Nat Rev Cancer* 2008;8:465-472.
9. Wakeford R, Little MP. Risk coefficients for childhood cancer after intrauterine irradiation: A review. *Int J Radiat Biol* 2003;79:293-309.
10. Di Majo V, Coppola M, Rebessi S, et al. Age-related susceptibility of mouse liver to induction of tumors by neutrons. *Radiat Res* 1990;124:227-234.
11. Mohr U. International Classification of Rodent Tumours. Part I: The Rat. 5. Integumentary Systems. Vol 122. Lyon: Oxford University Press; 1993.
12. Guigon CJ, Mazaud S, Forest MG, et al. Unaltered development of the initial follicular waves and normal pubertal onset in female rats after neonatal deletion of the follicular reserve. *Endocrinology* 2003;144:3651-3662.
13. Preston DL, Cullings H, Suyama A, et al. Solid cancer incidence in atomic bomb survivors exposed in utero or as young children. *J Natl Cancer Inst* 2008;100:428-436.
14. Russo J, Tay LK, Russo IH. Differentiation of the mammary gland and susceptibility to carcinogenesis. *Breast Cancer Res Treat* 1982;2:5-73.
15. Terato H, Tanaka R, Nakaarai Y, et al. Quantitative analysis of isolated and clustered DNA damage induced by gamma-rays, carbon ion beams, and iron ion beams. *J Radiat Res* 2008;49:133-146.
16. Jeggo PA, Geuting V, Lobrich M. The role of homologous recombination in radiation-induced double-strand break repair. *Radiother Oncol* 2011;101:7-12.
17. Shimada Y, Yasukawa-Barnes J, Kim RY, et al. Age and radiation sensitivity of rat mammary clonogenic cells. *Radiat Res* 1994;137:118-123.
18. Inskip PD, Robison LL, Stovall M, et al. Radiation dose and breast cancer risk in the childhood cancer survivor study. *J Clin Oncol* 2009;27:3901-3907.
19. Frank SJ. Mechanistic aspects of crosstalk between GH and PRL and ErbB receptor family signaling. *J Mammary Gland Biol Neoplasia* 2008;13:119-129.
20. Yonai S, Matsufuji N, Namba M. Calculation of out-of-field dose distribution in carbon-ion radiotherapy by Monte Carlo simulation. *Med Phys* 2012;39:5028-5039.

Published online 3 October 2011

Nucleic Acids Research, 2012, Vol. 40, No. 3 ***1065–1076***
doi:10.1093/nar/gkr805

Asymmetric nature of two subunits of RAD18, a RING-type ubiquitin ligase E3, in the human RAD6A–RAD18 ternary complex

Yuji Masuda[1,*], Miki Suzuki[1], Hidehiko Kawai[2], Fumio Suzuki[2,3] and Kenji Kamiya[1]

[1]Department of Experimental Oncology, [2]Department of Molecular Radiobiology and [3]Department of International Radiation Emergency Medicine, Research Institute for Radiation Biology and Medicine, Hiroshima University, 1-2-3 Kasumi, Minami-ku, Hiroshima 734-8553, Japan

Received May 31, 2011; Revised September 7, 2011; Accepted September 13, 2011

ABSTRACT

RAD18, a RING-type ubiquitin ligase (E3) that plays an essential role in post-replication repair, possesses distinct domains named RING, UBZ, SAP and the RAD6-binding domain (R6BD) and forms a dimer. RAD6, an ubiquitin-conjugating enzyme (E2), stably associates with R6BD in the C-terminal portion. In this study, we established a method to distinguish between the two subunits of RAD18 by introduction of different tags, and analyzed mutant complexes. Our results, surprisingly, demonstrate that RAD6A and RAD18 form a ternary complex, RAD6A–$(RAD18)_2$ and the presence of only one R6BD in the two RAD18 subunits is sufficient for ternary complex formation and the ligase activity. Interestingly, ligase activity of a mutant dimer lacking both R6BDs is not restored even with large amounts of RAD6A added in solution, suggesting a requirement for precise juxtaposition via interaction with R6BD. We further show that mutations in both subunits of either RING or SAP, but not UBZ, strongly reduce ligase activity, although inactivation in only one of two subunits is without effect. These results suggest an asymmetric nature of the two RAD18 subunits in the complex.

INTRODUCTION

Ubiquitin ligases (E3s) catalyze the transfer of ubiquitin from E2 (ubiquitin-conjugating enzyme)–ubiquitin conjugates to lysine residues in target proteins. A subset of E3s contains a RING (*r*eally *i*nteresting *n*ew *g*ene) domain, which binds to E2–ubiquitin conjugates and seems to activate thioester bonds (1,2). Some RING-type E3s are known to form heterodimers such as BRCA1–BARD1 (3–5), Ring1b-Bmi1 (6,7) and MDM2–MDMX (8–10), while others like cIAP2 (11) and RNF4 (12) act as homodimers. The heterodimeric RING-type E3s are composed of active and inactive RING domains, and dimerization enhances the ligase activity, suggesting that the pairing itself is very important for enzyme function (5,6,9).

Through a RAD6-binding domain (R6BD) located in its C-terminal region, the RAD18 RING-type ubiquitin ligase forms a stable complex with a specific E2, RAD6 (13–17). Since RAD6 also contacts the RING domain near the N-terminal of RAD18 for catalytic function (2,15,18), it could interact with two distinct domains of RAD18 simultaneously. Such interactions between an E2 and an E3 are quite unique to RAD6–RAD18. Recently, it has been reported that interaction between R6BD and RAD6 blocks the intrinsic activity of RAD6 in forming ubiquitin chains, ensuring mono-ubiquitination of PCNA (19). Previous studies have also reported that RAD18 forms a dimer and suggested the RAD6–RAD18 complex to be a dimer of RAD6–RAD18 heterodimer (15,20,21), hereafter designated as $(RAD6–RAD18)_2$.

RAD6 and RAD18 play an essential role in post-replication repair of damaged DNA *via* ubiquitination of proliferating cell nuclear antigen (PCNA) at Lys164 (22,23). The RAD6–RAD18 complex itself catalyzes mono-ubiquitination of PCNA *in vitro* (24–28). The mono-ubiquitinated PCNA appears to enhance lesion bypass replication by stimulation of entry of translesion DNA polymerases at stalled 3′-ends, through interactions between ubiquitin-binding domains of the polymerases and ubiquitin moieties of mono-ubiquitinated PCNA (24,26,29–31). Furthermore, RAD18 features a pol η-binding domain that is important for recruiting pol η to stalled 3′-ends (17,32).

RAD18 has two other domains UBZ (ubiquitin-binding zinc finger) (33–35) and SAP (*S*AF-A/B, *A*cinus and

*To whom correspondence should be addressed. Tel: +81 82 257 5893; Fax: +81 82 257 5843; Email: masudayu@hiroshima-u.ac.jp

PIAS) (15,36–38). The former is required for accumulation of RAD18 at damage sites (34,37,39) and has affinity for Ub chains (33,34) suggesting specific binding to damage-associated poly-ubiquitinated proteins (39). The SAP domain possesses DNA-binding activity (15,38), although it appears to be unnecessary for accumulation of RAD18 at damage sites (37,39). Rather, it is crucial for pol η focus formation (37) possibly depending on PCNA ubiquitination, which is attributed to an essential role of the SAP domain in ligase activity (38,39).

Although multiple domains of RAD18 are clearly concerned with ligase activity, it is unknown how the distinct entities of the two RAD18 subunits interact with each other for enzyme function. In the present study, we established a method to analyze the structure and functions of the human RAD6A–RAD18 complex and demonstrated an asymmetric nature of the two RAD18 molecules in the complex.

MATERIALS AND METHODS

Plasmids

Expression plasmids for RAD6A–RAD18, E1, ubiquitin, PCNA and RFC were as described previously (26,40–42). For overproduction of human RAD6A, RAD6A–^{His}RAD18, ^{FLAG}RAD6A–^{His}RAD18, the genes were cloned into pET20b(+) (Novagen) to yield pET-RAD6A and pET-RAD6A/hisRAD18, pET-flagRAD6A/hisRAD18, respectively. To make an expression plasmid compatible with pET plasmids in *Escherichia coli* cells, the entire coding unit of pET-RAD6A/RAD18 (42) was cloned into pACYC Duet1 (Novagen) to yield pAC-RAD6A/RAD18. Expression plasmids for overproduction of RAD6A–^{FLAG}RAD18 and ^{FLAG}RAD6A–^{FLAG}RAD18, pAC-RAD6A/flagRAD18 and pAC-flagRAD6A/flagRAD18 were generated, respectively. In those plasmids, His-tagged sequences were taken from pET15 and all tagged sequences were attached to immediately before the start codons of the respective genes. Expression plasmids in human cells for *RAD6* were cloned in pCMV, and for *RAD18* in pCDNA3 flag and pCAGGS (43).

Proteins

Proteins used in this study were overproduced in *E. coli* cells. During all purification steps, monitoring was done by SDS–PAGE followed by staining with Coomassie Brilliant Blue R-250 (CBB), or western blotting. Protein concentrations were determined by Bio-Rad protein assay using BSA (Bio-Rad) as the standard. PCNA, RFC, E1, ubiquitin and RAD6A–RAD18 complex were purified as described previously (26,40,41). Detailed procedures for purification of recombinant proteins established in this study are described in Supplementary Data.

Sucrose density gradient sedimentation

Sucrose density gradient sedimentation was performed as described earlier (44). Purified RAD6A–RAD18 complexes (1.7 μg), were sedimented through 2 ml of 10–40% sucrose gradient in buffer A containing 300 mM NaCl by centrifugation at 55 000 rpm for 20 h in a TLS 55 rotor (Beckman) at 4°C and fractions (100 μl) were collected from the bottom of the tube and analyzed by SDS–PAGE. Gel bands were stained with CBB and quantified using Multi Gauge software Version 3.0 (FUJIFILM). Sedimentation coefficients were determined relative to those of standard proteins sedimented in parallel gradients.

Antibodies

To obtain polyclonal antibodies against RAD18, truncated His-tagged RAD18 proteins (127–255 amino acids) were expressed in BL21 (DE3) (45), purified and used to immunize rabbits. Anti-Penta-His monoclonal (Qiagen, 34660), anti-FLAG M2 monoclonal (Sigma, F3165), anti-RAD6 polyclonal (Abcam, ab31917) and anti-PCNA polyclonal (Santa Cruz, sc-7907) antibodies were purchased.

PCNA-mono-ubiquitination assays

The standard reaction mixture (25 μl) contained 20 mM HEPES–NaOH (pH 7.5), 50 mM NaCl, 0.2 mg/ml BSA, 1 mM DTT, 10 mM $MgCl_2$, 1 mM ATP, 100 ng poly(dA)-oligo(dT), PCNA (1 pmol), RFC (350 fmol), E1 (850 fmol), ubiquitin (170 pmol) and the indicated amounts of RAD6A–RAD18 complex. Reaction mixtures were prepared on ice then incubated at 30°C for 10 min. The reactions were terminated by addition of 2× SDS sample buffer containing 25 mM EDTA. Ubiquitination of PCNA was assessed by western analysis, detected by an ECL chemiluminescence kit (GE Healthcare Life Science).

RESULTS

Physicochemical properties of the human RAD6A–RAD18 complex

To study the subunit composition of RAD6A–RAD18 complex, we first determined the Stokes' radius and sedimentation coefficient of the purified RAD6A–RAD18 complex (26) by gel filtration and sucrose density gradient centrifugation, respectively (Table 1). The obtained value of Stokes' radius (62 Å) corresponds to an apparent molecular mass of 490 kDa, but that of the

Table 1. Physicochemical properties of the RAD6A–RAD18 complex

Stokes' radius[a] (Å)	Sedimentation coefficient[b] × 10^{-13} s ($S_{20,w}$)	Molecular mass[c] (kDa)
62	5.0	131

[a]Determined by Superdex 200 gel filtration using the size markers ferritin (61.0 Å), aldolase (48.1 Å), albumin (35.5 Å) ovalbumin (30.5 Å) and ribonuclease A (16.4 Å), and the data were based on A_{280} values monitored during the chromatography.
[b]Determined with ferritin (17.6 S), catalase (11.3 S), aldolase (7.4 S), albumin (4.2 S) and ribonuclease A (1.8 S) as standards, and the data were based on the SDS–PAGE gel profile.
[c]Estimated from the Stokes' radius and the sedimentation coefficient assuming a partial specific volume of 0.73 (46).

sedimentation coefficient (5.0 S) corresponds to an apparent molecular mass of 70 kDa. The large difference between these two values suggests that the complex does not have a compact globular shape. Employing the method described by Siegel and Monty (46), we estimated the molecular mass of the RAD6A–RAD18 complex to be 131 kDa (Table 1). Since calculated molecular masses of RAD6A and RAD18 are 17.3 and 56.2 kDa, respectively, the total of molecular mass should be 73.5 kDa for RAD6A–RAD18 and 147 kDa for $(RAD6A–RAD18)_2$. Although the value estimated from the experiments was close to that of $(RAD6A–RAD18)_2$, we further investigated the stoichiometry of RAD6A and RAD18 in the complex.

Direct evidence that the RAD6A–RAD18 complex contains two RAD18 molecules

To obtain direct evidence that the RAD6A–RAD18 complex contains two molecules of RAD18, we co-expressed both His-tagged *RAD18* and FLAG-tagged *RAD18* genes together with *RAD6A* gene in the same *E. coli* cells. Three different complexes containing ^{His}RAD18–^{His}RAD18, ^{FLAG}RAD18–^{FLAG}RAD18 or ^{His}RAD18–^{FLAG}RAD18 would be expected if we assume that the complex should contain two molecules of RAD18. When the cell lysate was loaded to a Ni-chelating column, we found some ^{FLAG}RAD18 to be absorbed to the column and eluted together with approximately equal amounts of ^{His}RAD18 at a lower imidazole concentration (Figure 1A, lane 2), whereas the remainder of the ^{His}RAD18 was eluted at a higher imidazole concentration (see Supplementary Materials and Methods section). Since it was expected that the former was ^{His}RAD18–^{FLAG}RAD18 hetero complex and the latter was ^{His}RAD18 homo complex, the former was further purified through a heparin column (Figure 1A, lane 3) and analyzed by gel filtration (Figure 1A, lane 4). The elution profile was the same as that of untagged

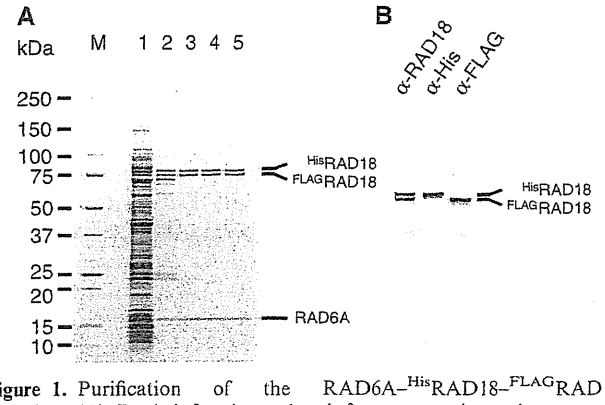

Figure 1. Purification of the RAD6A–^{His}RAD18–^{FLAG}RAD18 complex. (**A**) Pooled fractions eluted from respective columns were analyzed by SDS–PAGE followed by staining with CBB. Lane 1, cell lysate; lane 2, Ni-chelating column; lane 3, heparin column; lane 4, gel-filtration column; lane 5, anti-FLAG affinity column. Molecular masses of each marker (lane M) are shown to the left of the gel. (**B**) Western analysis of the pooled fraction eluted from the gel filtration column. Membranes were probed with the indicated antibodies.

RAD6A–RAD18 complex (Table 1 and see also Figure 6C), suggesting the tag sequences do not affect the overall structure of the complex. While western blotting with anti-Penta-His and anti-FLAG antibodies specifically detected ^{His}RAD18 and ^{FLAG}RAD18 proteins, respectively (Figure 1B), blotting with anti-RAD18 antibodies detected the two proteins equally, thereby indicating that the purified complex contains ^{His}RAD18 and ^{FLAG}RAD18 at a 1:1 ratio. To further verify that RAD6A, ^{His}RAD18 and ^{FLAG}RAD18 form a complex, a fraction eluted from gel filtration was applied to FLAG-affinity chromatography. The result demonstrated that the three proteins were adsorbed to the anti-FLAG M2 affinity gel and eluted with the FLAG peptide (Figure 1A, lane 5). We thus conclude that the RAD6A–RAD18 complex contains two RAD18 molecules.

Subunit composition of the RAD6A–RAD18 complex is RAD6A–$(RAD18)_2$

To examine the stoichiometry of RAD6A in the complex, we directly compared amounts of RAD6A in the complex with purified RAD6A protein as a reference. We applied 500 ng of the purified complex, RAD6A–^{His}RAD18–^{FLAG}RAD18, in parallel with different amounts (65 or 115 ng) of RAD6A monomers to SDS–PAGE. The amounts of RAD6A in the complex should be 65 or 115 ng, if the complex is RAD6A–$(RAD18)_2$ or $(RAD6A–RAD18)_2$, respectively (Figure 2A). The results of CBB staining and western blotting showed the amount of RAD6A in the complex to be closer to 65 ng (Figure 2A), thus suggesting that the complex contains RAD6A and RAD18 at the ratio of 1:2. To confirm this, the FLAG-tag was introduced to RAD6A and the ^{FLAG}RAD6A–^{His}RAD18–^{FLAG}RAD18 complex was purified as described above. We applied 505 ng of the purified complex to SDS–PAGE, in parallel with 500 ng of RAD6A–^{His}RAD18–^{FLAG}RAD18 as a reference (Figure 2B). Western blotting with anti-RAD6 antibodies confirmed that both complexes contained equivalent amounts of RAD6A (Figure 2B), and blotting with an anti-FLAG antibody clearly demonstrated that the molecular ratio of ^{FLAG}RAD6A and ^{FLAG}RAD18 was 1:1 (Figure 2B), suggesting strongly the ratio of RAD6A to RAD18 to be 1:2.

R6BD is located within amino acid residues 340–395 of RAD18 (Figure 3D) (17,19). Using a deletion mutant consisting of amino acid residues 1–341 of RAD18 (hereafter designated as $RAD18^{\Delta CI}$, Figure 3D), we further examined the stoichiometry of RAD6 and RAD18. When $^{His}RAD18^{\Delta CI}$ and $^{FLAG}RAD18^{\Delta CI}$ were co-produced with RAD6A in the same *E. coli* cells, a complex containing $^{His}RAD18^{\Delta CI}$ and $^{FLAG}RAD18^{\Delta CI}$ was purified similarly as described above, but it did not contain RAD6A (Figure 2C, lane 3). This result indicates that the R6BD is required for complex formation with RAD6 but is dispensable for dimerization. In contrast, when $^{His}RAD18^{\Delta CI}$ was co-produced with ^{FLAG}RAD18 and RAD6A in the same *E. coli* cells, we successfully obtained a RAD6A–$^{His}RAD18^{\Delta CI}$–^{FLAG}RAD18 ternary complex

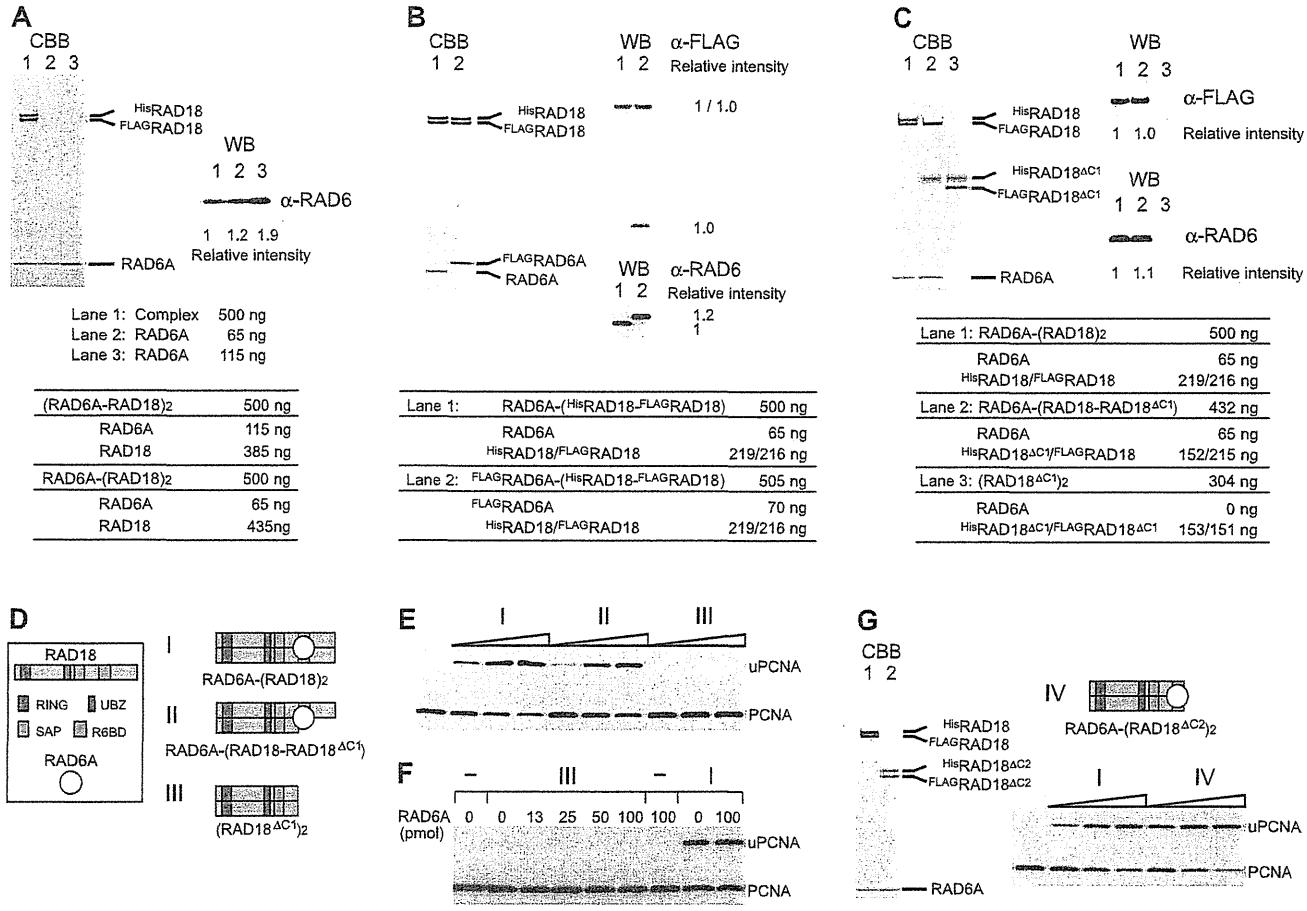

Figure 2. Subunit composition of the RAD6A–RAD18 complex and deletion analysis of RAD18. (**A**) The indicated amounts of purified RAD6A–RAD18 complex and RAD6A were analyzed by SDS–PAGE followed by staining with CBB and western blotting probed with anti-RAD6 antibodies. Relative chemiluminescence signals detected with a CCD camera are shown. Amounts of each subunit calculated for two different postulated subunit compositions are shown in the table. (**B** and **C**) Indicated amounts of purified RAD6A–RAD18 complexes were analyzed by SDS–PAGE followed by staining with CBB and western blotting probed with anti-FLAG and anti-RAD6 antibodies. Relative chemiluminescence signals detected with a CCD camera are shown. Amounts of each subunit calculated for the postulated subunit compositions are shown in the tables. (**D**) Schematic representations of the structures for respective RAD6A–RAD18 complexes. (**E**) Ligase activities of the respective RAD6A–RAD18 complexes. Increasing amounts of the complexes (0.5, 1 and 2 pmol) were subjected to standard assays. The reaction products were analyzed by western blotting with anti PCNA antibodies. I, RAD6A–(^{His}RAD18–^{FLAG}RAD18); II, RAD6A–(^{His}RAD18$^{\Delta C1}$–^{FLAG}RAD18); III, ^{His}RAD18$^{\Delta C1}$–^{FLAG}RAD18$^{\Delta C1}$. (**F**) Titration of RAD6A in the reaction with ^{His}RAD18$^{\Delta C1}$–^{FLAG}RAD18$^{\Delta C1}$. Indicated amounts of RAD6A were incubated with 2 pmol of ^{His}RAD18$^{\Delta C1}$–^{FLAG}RAD18$^{\Delta C1}$ (III) under standard assay conditions. As control reactions, 1 pmol of RAD6A–(^{His}RAD18–^{FLAG}RAD18) (I) was incubated in the presence or absence of additional RAD6A. (**G**) Analysis of complex formation and ligase activity of another C-terminal deletion mutant of RAD18. Purified complexes (3.7 pmol as a trimer) were analyzed by SDS–PAGE followed by staining with CBB. Lane 1, RAD6A–(^{His}RAD18–^{FLAG}RAD18) (I); lane 2, RAD6A–(^{His}RAD18$^{\Delta C2}$–^{FLAG}RAD18$^{\Delta C2}$) (IV). Structure of the mutant complex (IV) was represented schematically. Assays were performed as described in (E).

(Figure 2C, lane 2), indicating that only one R6BD in the two RAD18 subunits could form the complex with RAD6A. Again, amounts of each protein in these complexes were compared by CBB staining and western blotting. For Figure 2C, we applied 500 ng of RAD6A–^{His}RAD18–^{FLAG}RAD18 (lane 1) and 432 ng of the RAD6A–^{His}RAD18$^{\Delta C1}$–^{FLAG}RAD18 complex (lane 2) to SDS–PAGE. If stoichiometry of each component were 1:1:1 in both complexes, amounts of each ^{FLAG}RAD18 and each RAD6A in the two complexes should be identical (Figure 2C). The results of CBB staining and western blotting proved to be in good agreement with our estimations (Figure 2C, lanes 1 and 2), suggesting that the RAD18 dimer, as well as the RAD18 monomer, is capable of accommodating only one RAD6 molecule (Figure 2D). Very interestingly, the hetero complex RAD6A–(^{His}RAD18$^{\Delta C1}$–^{FLAG}RAD18) was catalytically active in terms of PCNA ubiquitination (Figure 2E). As expected, ^{His}RAD18$^{\Delta C1}$–^{FLAG}RAD18$^{\Delta C1}$ was inactive (Figure 2E), and its ligase activity was hardly restored by addition of excess amounts of RAD6A in solution (Figure 2F). To see whether the defect is due to the loss of function of the C-terminal portion, another truncated RAD18 mutant consisting of amino acid residues 1–388 (hereafter designated as RAD18$^{\Delta C2}$, Figure 3D), was examined. It was expected that RAD18$^{\Delta C2}$ could form a

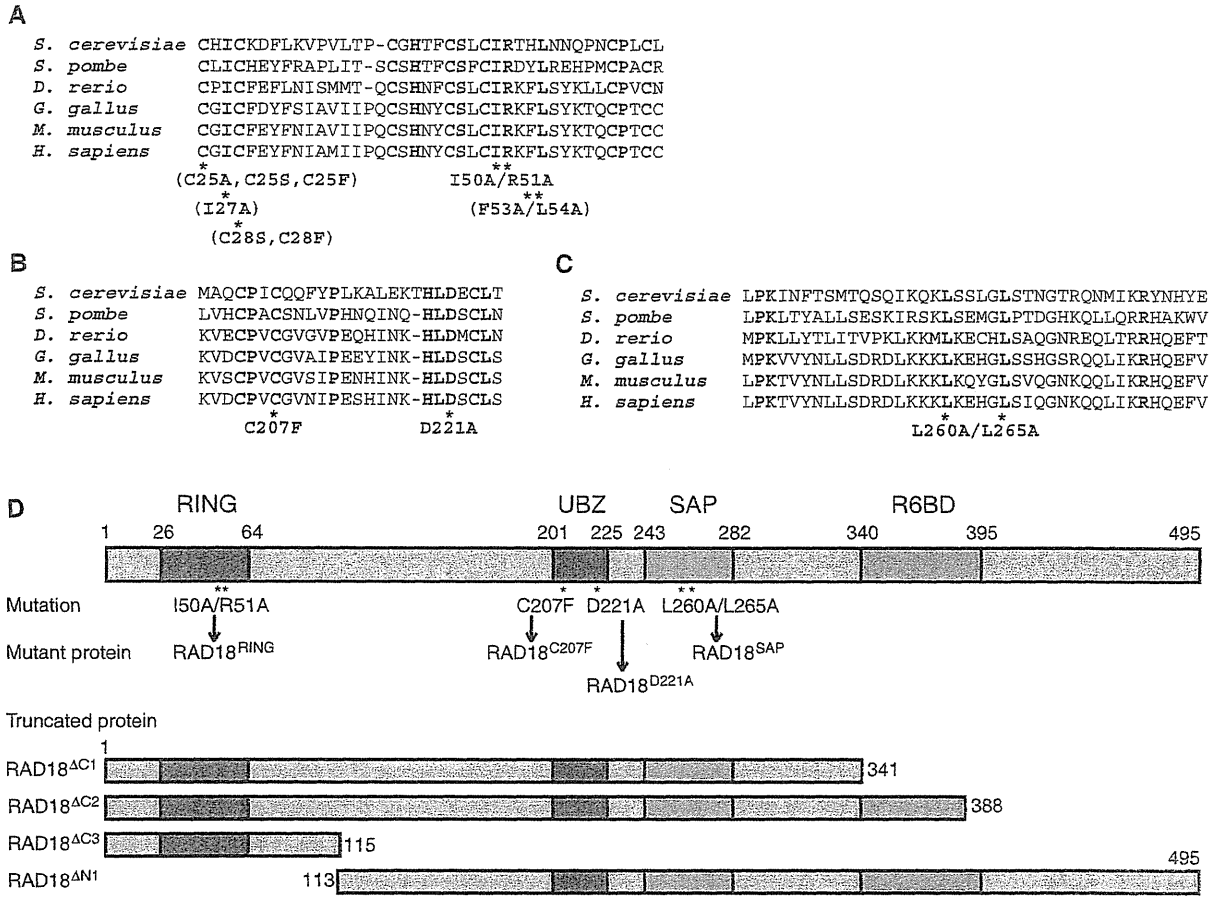

Figure 3. RAD18 mutants analyzed in this study. (**A**) Multiple alignments of the RING domains of human RAD18 and its orthologs. Mutants analyzed in this study are shown below the alignments. Mutants shown in parentheses were eluted in void volumes of gel filtration chromatography. (**B**) Multiple alignments of UBZ of human RAD18 and its orthologs. (**C**) Multiple alignments of the SAP domains of human RAD18 and its orthologs. (**D**) Schematic representations of the structures of RAD18. Positions of the mutations are shown with designated names of the mutant proteins.

complex with RAD6, since it retained R6BD (Figure 3D) (15). Indeed, it was successfully reconstituted into a ternary complex, RAD6A–^{His}RAD18$^{\Delta C2}$_^{FLAG}RAD18$^{\Delta C2}$, and the complex exhibited ligase activity similar to the wild-type level (Figure 2G), indicating that the C-terminal region of 389–495 amino acid residues is dispensable for ligase activity. From all these results (Figures 1 and 2), together with the fact that RAD6 is essentially a monomer (see Supplementary Materials and Methods section) (19,47), we conclude the subunit composition of the RAD6A–RAD18 complex to be RAD6A–(RAD18)$_2$ with a molecular mass of 130 kDa. Thus, the overall structure of the complex is asymmetric. Notably, this well matched the 131 kDa estimated molecular mass from the Stokes' radius and the sedimentation coefficient (Table 1).

Evidence of the ternary complex, RAD6A–(RAD18)$_2$, *in vivo*

To obtain evidence of ternary complex formation *in vivo*, HA-tagged *RAD6A* and FLAG-tagged *RAD18* were expressed together in human cells, and ^{HA}RAD6A–^{FLAG}RAD18 complexes were isolated using FLAG affinity and then HA affinity gels. The complexes were a mixture of unmodified RAD18 and mono-ubiquitinated RAD18, as reported previously (Figure 4A) (48). Subunit composition of the purified complexes was determined by western blotting with anti-RAD6 and anti-RAD18 antibodies using RAD6A–(RAD18)$_2$ complex purified from *E. coli* cells (26) as references. Ratio of signals from ^{HA}RAD6A and ^{FLAG}RAD18 well fitted those from RAD6A–(RAD18)$_2$ complexes (Figure 4A), suggesting the subunit composition to be RAD6A–(RAD18)$_2$. This was further confirmed using partially purified untagged RAD6A–RAD18 complexes generated by conventional column chromatography from *RAD6A* and *RAD18* expressing human cells. We found that RAD6A, RAD18 and mono-ubiquitinated RAD18 all eluted together from a gel filtration column (Figure 4B), similar to the RAD6A–(RAD18)$_2$ complex (Table 1 and Figure 6C). Again, the subunit composition of the eluted fraction corresponded to RAD6A–(RAD18)$_2$ (Figure 4B). These results strongly suggest ternary complex formation *in vivo*.

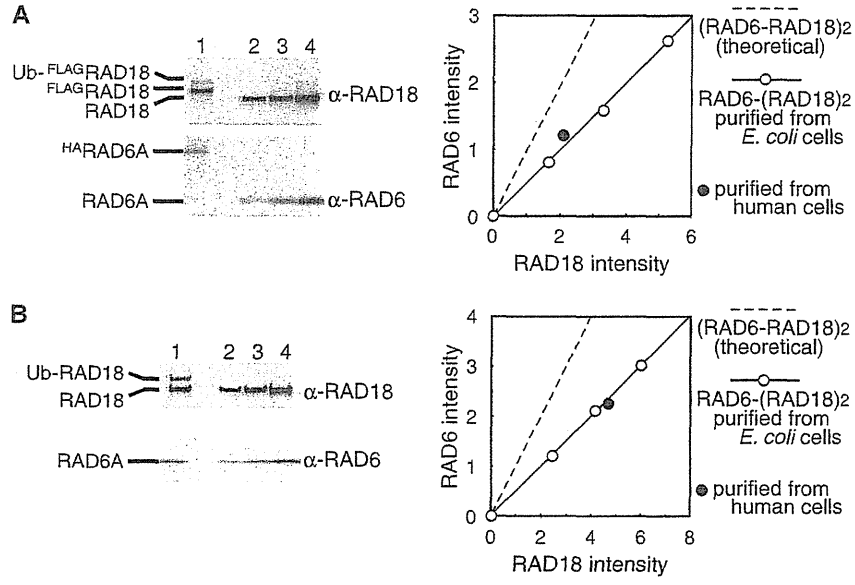

Figure 4. Ternary complex formation of RAD6A and RAD18 *in vivo*. (**A**) ^{HA}RAD6–^{FLAG}RAD18 complexes isolated from human cells were analyzed by SDS–PAGE (lane 1) together with RAD6A–(RAD18)$_2$ isolated from *E. coli* (lanes 2–4) followed by western blotting probed with anti-RAD18 and anti-RAD6 antibodies. Relative chemiluminescence signals of ^{HA}RAD6A and ^{FLAG}RAD18 (sum of unmodified ^{FLAG}RAD18 and Ub-^{FLAG}RAD18) detected with a CCD camera were plotted with those of RAD6A and RAD18 purified from *E. coli* as references. The theoretical 1:1 ratio of RAD6 and RAD18 is shown as a broken line. (**B**) Untagged RAD6–RAD18 complexes isolated from human cells were analyzed by SDS–PAGE as (A).

Analysis of UBZ roles in complex formation and ligase activity

Our system to purify RAD6–RAD18 complex with two different tags is a useful tool for analysis of structure–function relationships in RAD18. First, we applied this system to test whether UBZ is required for dimerization of RAD18 using two loss-of-function mutants, RAD18^{C207F} and RAD18^{D221A} (34,37) (Figure 3B and D). The results demonstrated that these mutants were successfully reconstituted into the complexes, RAD6A–(RAD18^{C207F})$_2$ and RAD6A–(RAD18^{D221A})$_2$ (Figure 5A) and their ligase activities were similar to that of wild-type complex (Figure 5B). These results indicate UBZ to be dispensable for complex formation and ligase activity, in line with recent reports (15,39), demonstrating reliability of our system for analysis of the structure and function of RAD6–RAD18 complexes.

Functional interaction between RAD6 and the RING domains of the two subunits of RAD18 in the complex

Next, we addressed the question whether the N-terminal part containing a RING domain mediates dimerization. We generated another truncated RAD18 mutant consisting of the 1–115 amino acid residues of RAD18 (hereafter designated as RAD18$^{\Delta C3}$, Figure 3D). When ^{His}RAD18$^{\Delta C3}$ and ^{FLAG}RAD18$^{\Delta C3}$ were co-produced with RAD6A in the same *E. coli* cells, we found the ^{His}RAD18$^{\Delta C3}$-^{FLAG}RAD18$^{\Delta C3}$ dimer to be reconstituted, but that RAD6A did not co-purify with the dimer. The observed elution profile of the dimer from a gel filtration column is shown in Figure 6A. ^{His}RAD18$^{\Delta C3}$ and ^{FLAG}RAD18$^{\Delta C3}$, confirmed by western blotting (Figure 6B), co-eluted with an apparent molecular mass of ~37 kDa, slightly larger than the calculated molecular mass of 29 kDa as a dimer (Figure 6A and B). As a complementary experiment, an N-terminal deletion mutant of RAD18 consisting of 113–495 amino acid residues (hereafter designated as RAD18$^{\Delta N1}$, Figure 3D), was generated. When ^{His}RAD18$^{\Delta N1}$ was coproduced with ^{FLAG}RAD18 and RAD6A, ^{His}RAD18$^{\Delta N1}$ co-purified with RAD6A but not with ^{FLAG}RAD18 (Figure 6D). As mentioned above, the RAD6A–(^{His}RAD18–^{FLAG}RAD18) ternary complex eluted at a position corresponding to 490 kDa in gel filtration (Figure 6C). In contrast, the complex of RAD6A–^{His}RAD18$^{\Delta N1}$ eluted at a position corresponding to 220 kDa, which is much smaller than the ternary complex (Figure 6C). Furthermore the molecular ratio of RAD6A and ^{His}RAD18$^{\Delta N1}$ determined by western blotting, compared with the ternary complex as a reference, was close to 1:1 (Figure 6D). These results suggest that the RAD6A–^{His}RAD18$^{\Delta N1}$ complex is a dimer composed of one RAD6A and one ^{His}RAD18$^{\Delta N1}$ molecule and imply that ^{His}RAD18$^{\Delta N1}$ neither self-associates nor forms a heterodimer with ^{FLAG}RAD18. From these data shown in Figure 6, we conclude that the N-terminal region (1–115) is necessary and sufficient for dimerization, while UBZ and SAP domains are dispensable.

In general, the RING domains of E3s have an essential function in ligase activity by mediating interactions with E2s (1,2). It is of great interest to clarify how the two RING domains interact with one RAD6 subunit in the RAD6A–(RAD18)$_2$ complex. To address this point, we made several mutants in which one or two conserved amino acid residues in the RING domain were replaced

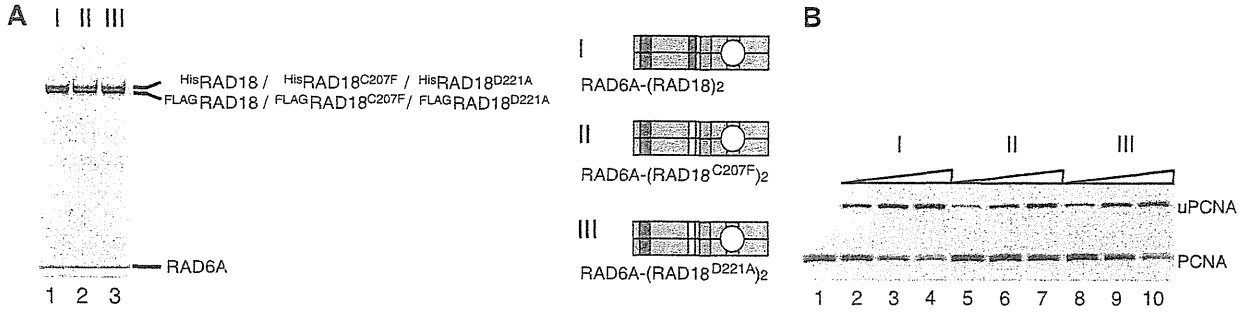

Figure 5. Analysis of ligase activity and complex formation with UBZ mutants of RAD18. (**A**) Purified complexes (3.7 pmol) were analyzed by SDS–PAGE followed by staining with CBB. I, RAD6A–(^{His}RAD18–^{FLAG}RAD18); II, RAD6A–(^{His}RAD18^{C207F}–^{FLAG}RAD18^{C207F}); III, RAD6A–(^{His}RAD18^{D221A}–^{FLAG}RAD18^{D221A}). Structures are represented schematically, UBZ domains with a mutation being shown in white boxes. (**B**) Ligase activity of the respective RAD6A–RAD18 complexes. Increasing amounts of the complexes (0.5, 1 and 2 pmol) shown in (A) were subjected to standard assays.

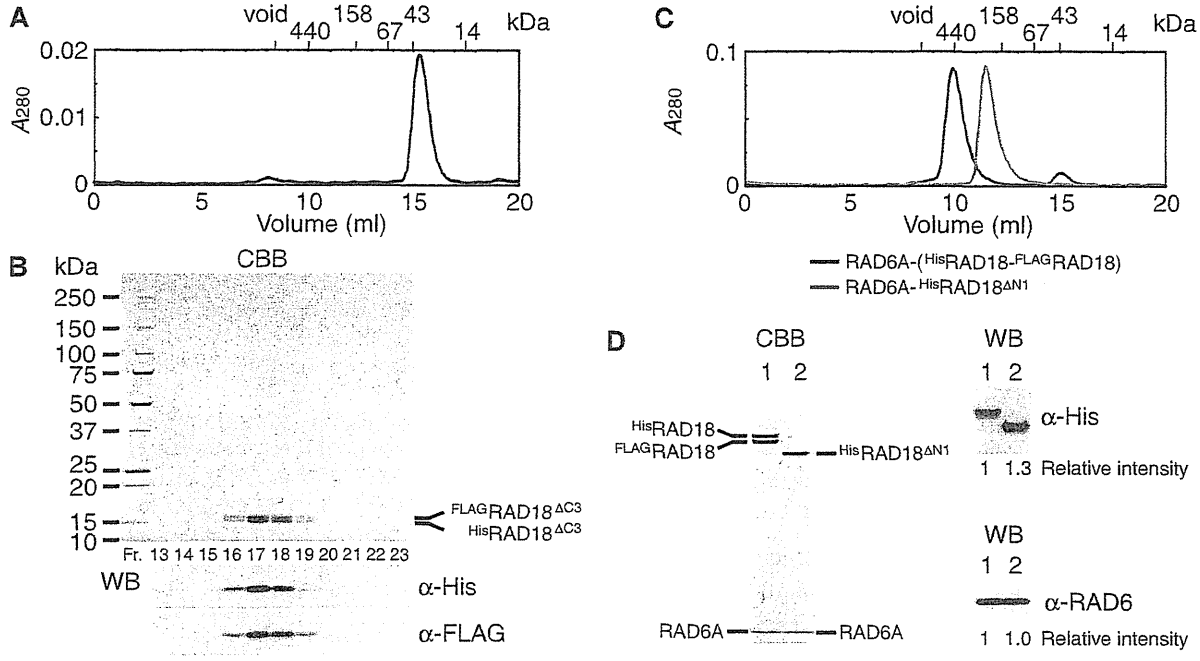

Figure 6. Analysis of RING domain for dimerization of RAD18. (**A**) Elution profile of ^{His}RAD18$^{\Delta C2}$–^{FLAG}RAD18$^{\Delta C2}$ complexes from a Superdex 200 gel filtration column. The size markers, ferritin (440 kDa), aldolase (158 kDa), albumin (67 kDa), ovalbumin (43 kDa) and ribonuclease A (14 kDa) were eluted in 10.09, 12.26, 13.74, 14.98 and 17.56 ml, respectively. The complex was eluted in 15.35 ml, estimated the apparent molecular mass of the complex to be 37 kDa from a standard curve of the marker proteins. (**B**) Analysis of fractions eluted from a Superdex 200 gel filtration column (A). Fractions between 13 and 18.5 ml were analyzed by SDS–PAGE followed by staining with CBB and western blotting probed with the indicated antibodies. ^{His}RAD18$^{\Delta C2}$ (15.1 kDa) migrated slightly faster than ^{FLAG}RAD18$^{\Delta C2}$ (14.2 kDa). (**C**) Elution profile of RAD6A–(^{His}RAD18–^{FLAG}RAD18) and RAD6A–^{His}RAD18$^{\Delta N1}$ complexes from a Superdex 200 gel filtration column. Respective complexes were eluted in 9.77 and 11.45 ml, corresponding to 490 and 220 kDa of the apparent molecular masses, and 62 and 52 Å of Stokes' radius, estimated from a standard curve of the marker proteins. (**D**) Peak fractions of gel filtration chromatography (C) were analyzed by SDS–PAGE followed by CBB staining and western blotting probed with the indicated antibodies. Relative chemiluminescence signals detected with a CCD camera are shown. Lane 1, RAD6A–(^{His}RAD18–^{FLAG}RAD18) (3.7 pmol as a trimer); lane 2, RAD6A–^{His}RAD18$^{\Delta N1}$ (3.7 pmol as a dimer).

as indicated in Figure 3A. We found that RING mutants with C25A, C25S, C25F, I27A, C28S, C27F or F53A/L54A substitutions eluted in void volumes on gel filtration chromatography, suggesting these mutants to form large aggregates due to highly disordered structures by misfolding. Therefore we did not further analyze them. However, we could successfully obtain one mutant complex containing I50A/R51A substitutions in RAD18 (hereafter designated as RAD18^{RING}, see Figures 3A and 7A, lane 2). A previous report suggested, based on the crystal structure of the c-Cbl-UbcH7 complex, that the amino acid residues Ile50 and Arg51 of RAD18 should be located in a predicted RAD6-interacting α-helix (2). Thus, it was expected that I50A/R51A mutations would affect

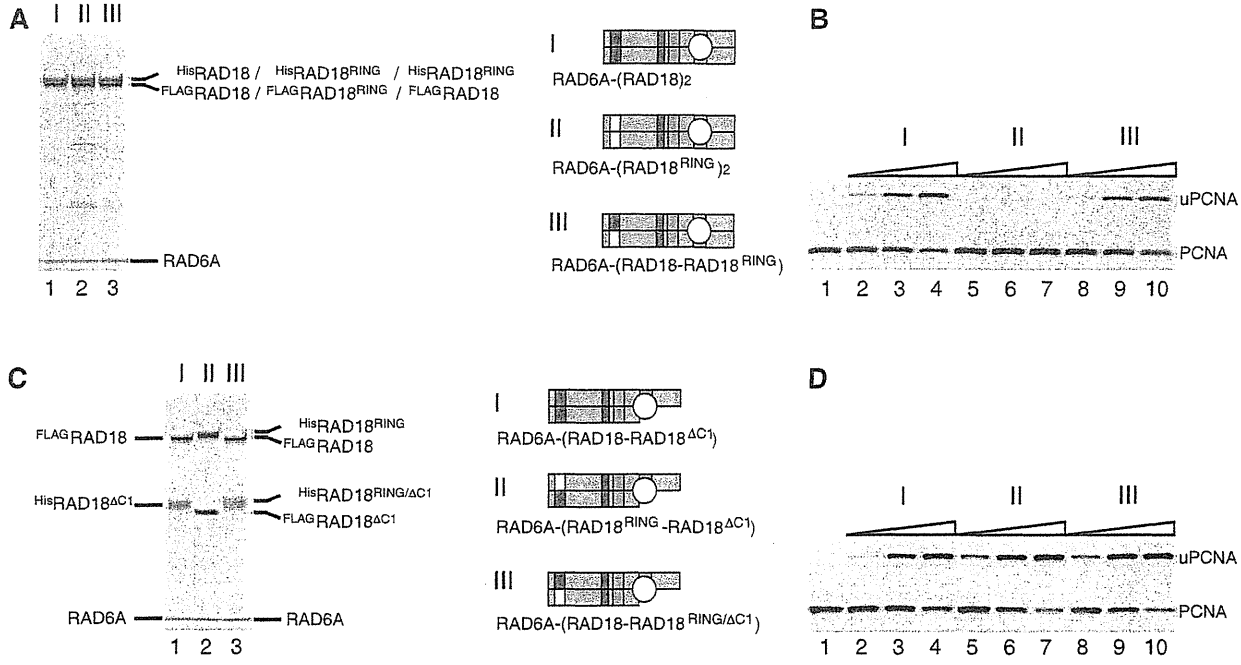

Figure 7. Analysis of ligase activity and complex formation of a RING mutant of RAD18. (**A**) Purified complexes (3.7 pmol) were analyzed by SDS–PAGE followed by staining with CBB. I, RAD6A–(^{His}RAD18–^{FLAG}RAD18); II, RAD6A–(^{His}RAD18^{RING_FLAG}RAD18^{RING}); III, RAD6A–(^{His}RAD18^{RING_FLAG}RAD18). Structures are represented schematically. RING domains with a mutation being shown in white boxes. (**B**) Ligase activities of the respective RAD6A–RAD18 complexes. Increasing amounts of the complexes (0.5, 1 and 2 pmol) shown in (A) were subjected to standard assays. (**C**) Purified complexes (3.7 pmol) were analyzed by SDS–PAGE followed by staining with CBB. I, RAD6A–(^{His}RAD18$^{\Delta C1_FLAG}$RAD18); II, RAD6A–(^{His}RAD18^{RING_FLAG}RAD18$^{\Delta C1}$); III. RAD6A–(^{His}RAD18$^{RING/\Delta C1_FLAG}$RAD18). (**D**) Ligase activities of the respective RAD6A–RAD18 complexes. Increasing amounts of the complexes (0.5, 1 and 2 pmol) shown in (C) were subjected to standard assays.

the ligase activity of RAD18. In fact, it was much reduced when compared to that of the wild-type complex (Figure 7B). Then, we reconstituted a hetero complex with the mutant and wild-type, RAD6A–(^{His}RAD18^{RING_FLAG}RAD18) (Figure 7A, lane 3). Surprisingly, its ligase activity was essentially identical to that of the wild-type (Figure 7B), indicating that an interaction between RAD6 and only one RING domain in the two RAD18 subunits is sufficient for ligase activity. In addition, I50A/R51A mutations were combined with the ΔC1 mutation and two mutant complexes, RAD6A–(^{His}RAD18^{RING_FLAG}RAD18$^{\Delta C1}$) and RAD6A–(^{His}RAD18$^{RING/\Delta C1_FLAG}$RAD18) were reconstituted (Figure 7C). Analysis of their ligase activities demonstrated these to be as active as the wild-type (Figure 7D), indicating that one RAD6 molecule in the complex has the potential to interact with either subunit of the RAD18 dimer.

Functional interaction between SAP and R6BD for ligase activity

It has been shown that the SAP domain of RAD18 has DNA-binding activity (15,38), which is separable from its essential function for ligase activity (38). When a mutant RAD18 containing L250A/L265A substitutions (hereafter designated as RAD18^{SAP}, see Figure 3D) was successfully reconstituted into the ternary complex, RAD6A–(^{His}RAD18^{SAP_FLAG}RAD18^{SAP}) (Figure 8A, lane 2), the ligase activity of the mutant complex was reduced to an undetectable level (Figure 8B). However, activity was restored in a hetero complex with the wild-type, RAD6A–(^{His}RAD18^{SAP_FLAG}RAD18) (Figure 8B), demonstrating that only one of the two SAP domains in the complex is sufficient for the essential SAP function. Next, the SAP mutation was combined with the ΔC1 mutation to reconstitute RAD6A–(^{His}RAD18^{SAP_FLAG}RAD18$^{\Delta C1}$) and RAD6–(^{His}RAD18$^{SAP/\Delta C1_FLAG}$RAD18) (Figure 8C). Interestingly, the former had quite reduced ligase activity, but the latter exhibited the wild-type level (Figure 8D), indicating that the active SAP domain should be present on the same RAD18 molecule to which RAD6 binds. In contrast, such functional interaction was not observed between RING and SAP mutants; ligase activities of RAD6A–(^{His}RAD18$^{RING/SAP_FLAG}$RAD18) and RAD6–(^{His}RAD18^{RING_FLAG}RAD18^{SAP}) complexes (Figure 8E) were similar to that of wild-type (Figure 8F).

DISCUSSION

In this study, we established a method to distinguish between the two subunits of RAD18 in the RAD6–(RAD18)$_2$ complex by introducing different tags at the N-termini. This enabled us to purify RAD18 complexes composed of wild–wild, wild–mutant or mutant–mutant subunits and facilitated analysis of structure–function relationships in RAD18.

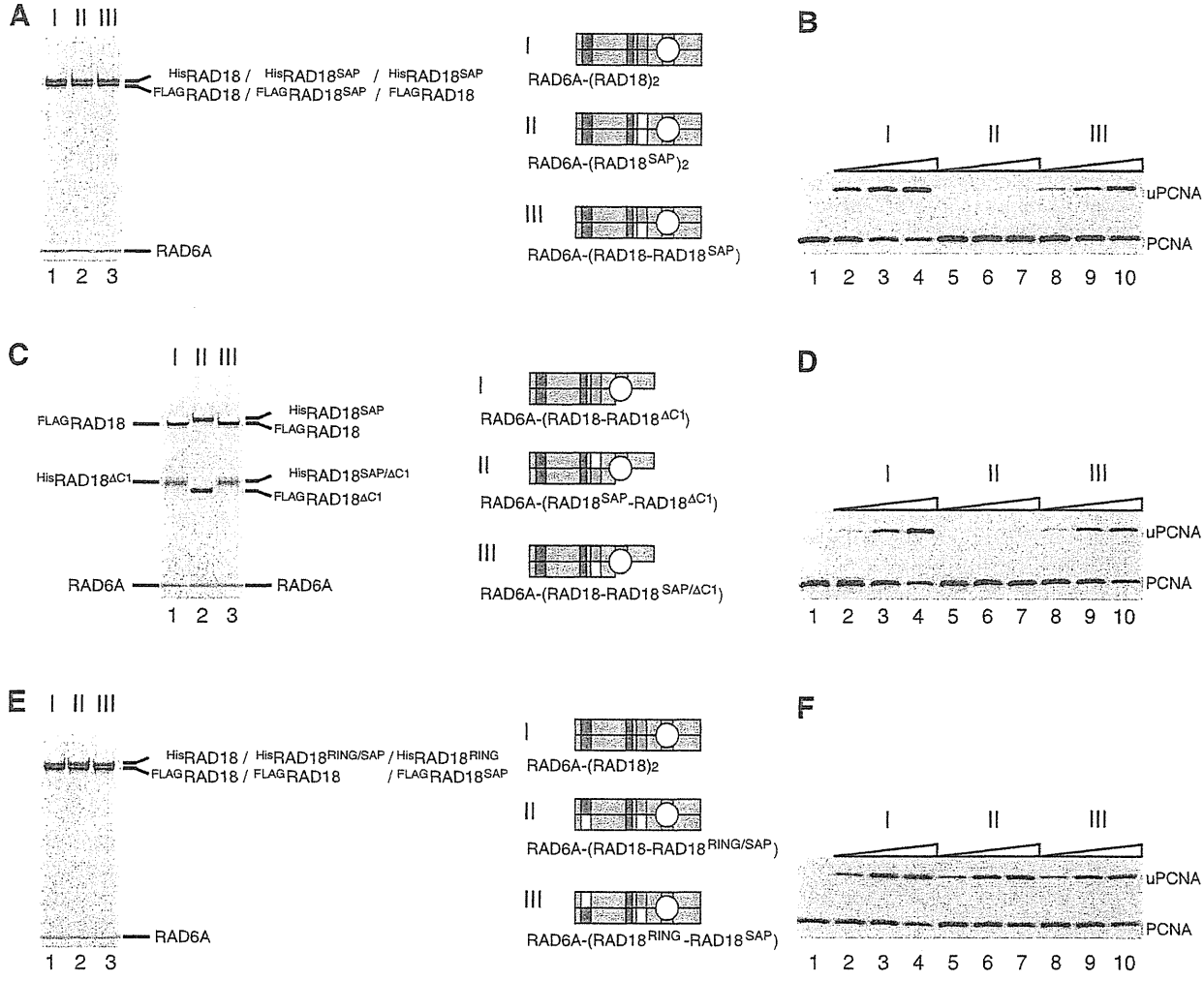

Figure 8. Analysis of ligase activity and complex formation of a SAP mutant of RAD18. (**A**) Purified complexes (3.7 pmol) were analyzed by SDS–PAGE followed by staining with CBB. I, RAD6A–(^{His}RAD18–^{FLAG}RAD18); II, RAD6A–(^{His}RAD18^{SAP}–^{FLAG}RAD18^{SAP}); III, RAD6A–(^{His}RAD18^{SAP}–^{FLAG}RAD18). Structures were represented schematically, SAP domains with a mutation being shown in white boxes. (**B**) Ligase activities of the respective RAD6A–RAD18 complexes. Increasing amounts of the complexes (0.5, 1 and 2 pmol) shown in (A) were subjected to standard assays. (**C**) Purified complexes (3.7 pmol) were analyzed by SDS–PAGE followed by staining with CBB. I, RAD6A–(^{His}RAD18$^{\Delta C1}$–^{FLAG}RAD18); II, RAD6A–(^{His}RAD18^{SAP}–^{FLAG}RAD18$^{\Delta C1}$); III, RAD6A–(^{His}RAD18$^{SAP/\Delta C1}$–^{FLAG}RAD18). (**D**) Ligase activities of the respective RAD6A–RAD18 complexes. Increasing amounts of the complexes (0.5, 1 and 2 pmol) shown in (C) were subjected to standard assays. (**E**) Purified complexes (3.7 pmol) were analyzed by SDS–PAGE followed by staining with CBB. I, RAD6A–(^{His}RAD18–^{FLAG}RAD18); II, RAD6A–(^{His}RAD18$^{RING/SAP}$–^{FLAG}RAD18); III, RAD6A–(^{His}RAD18^{RING}–^{FLAG}RAD18^{SAP}). (**F**) Ligase activities of the respective RAD6A–RAD18 complexes. Increasing amounts of the complexes (0.5, 1 and 2 pmol) shown in (E) were subjected to standard assays.

Previously, it was considered that the RAD6–RAD18 complex could be composed of two RAD6 and two RAD18, since the observations that RAD18 binds to RAD6 and it forms a dimer led to the assumption that each RAD18 molecule in the dimer should bind to RAD6 (15,20,21). However, there is little evidence for such an assignment based on the stoichiometry of RAD6. In this study, we provided hard lines of evidence that the complex is composed of one subunit of RAD6 and two subunits of RAD18, so that the overall structure of the ternary complex should be asymmetric.

The RING domains in E3s have an essential function in ligase activity by mediating interactions with E2s. Zheng *et al.* (2) have suggested, on the basis of the crystal structure of the c-Cbl-UbcH7 complex, that amino acid residues I50 and R51 in the RING domain of RAD18 are located in a predicted RAD6-interacting α-helix. Consistent with this, a mutant complex containing I50A/R51A substitutions in both RAD18 subunits exhibited severely reduced ligase activity, probably due to an impaired interaction between the altered RING domain and RAD6A. When the mutant subunit was complexed with wild-type RAD18 subunit, ligase activity was restored to the wild-type level, indicating that only one of the two RING domains is necessary for enzyme function. Furthermore, even when the RING mutation

was combined with a deletion mutation of R6BD in the same or other RAD18 subunit, the complexes exhibited robust ligase activity. These results imply that RAD6 can bind in either one of the two R6BDs, then interacting with one of the two RING domains in the RAD18 dimer.

Why should the RING domain of RAD18 form a dimer? We found that inactivation of one RING domain does not affect the ligase activity, indicating that the close proximity of two active RING domains in RAD18 is not important for the enzyme function. From our observations that some RING mutants such as C25A, C25S, C25F, I27A, C28S, C28F and F53A/L54A, probably disrupting the RING structure (Figure 3D), appeared to form large aggregates, we suggest that the RING structure is required for stable dimerization, which is in turn necessary for sustaining the functionally active RING structure of RAD18. From the results, we cannot exclude the possibility of retention of some enzyme functions even in aggregates. Indeed, it has been reported that the C28F mutant can fully complement the homologous recombination defects of RAD18-null cells (39).

The SAP domain is a unique eukaryotic module involved in sequence- or structure-specific DNA binding (36,38,49–52). Additionally, in RAD18 it has an essential role in ligase activity, separable from its function in DNA binding (38). We further demonstrated that one of the two SAP domains in the RAD6–$(RAD18)_2$ complex is sufficient for ligase activity. Interestingly, experiments using hetero complexes, in which mutation in the SAP domain was combined with a deletion mutation of R6BD, revealed an interesting relationship between SAP and R6BD. Although one of the two SAP domains and one of the two R6BDs are sufficient for enzyme activity, the active SAP domain should be present on the same RAD18 molecule to which RAD6 binds in the complex. It makes a sharp contrast to the case of RING mutant as described above. A simple explanation is that the SAP domain acts as a hinge connecting the R6BD and RING domain to enable precise juxtaposition between RING and RAD6. This might be very important for ligase activity because a deletion mutant of R6BD hardly supported PCNA ubiquitination in the presence of an excess amount of RAD6A, which should be high enough to detect ligase activities for many other E2–E3 pairs (4–6,9–2). It seems likely that binding affinity between RAD6 and the RING domain of RAD18 is very low. That could be the reason why R6BD is essential for ligase activity of the RAD6–RAD18 complex. The tight interaction between RAD6 and R6BD confers on the complex the ability to monoubiquitinate PCNA, also inhibiting the activity of RAD6 catalyzing ubiquitin chain formation (19).

In the above, we have shown that RAD6 and RAD18 forms a ternary complex, RAD6–$(RAD18)_2$ and demonstrated that one R6BD site is sufficient for the ligase activity. Then, a question that immediately arises is why RAD6 can bind to one of the two R6BD sites, but not to both of them. Although we have no experimental data to answer the question at the moment, such a case is not unprecedented. CHIP (*C*-terminal of *H*sp70 *i*nteracting *p*rotein), a protein containing a C-terminal Ubox domain (similar to RING) and an N-terminal TPR domain, forms an asymmetric dimer mediated by the Ubox domains, in which only one of the two Ubox domains is available for binding to E2 (Ubc13) because the other Ubox domain is blocked due to interaction with the TPR domain (53). It is tempting to speculate that a segment including R6BD located in a C-terminal portion of the two RAD18 subunits may interact with one of the two RING domains, consequently preventing the R6BD from interacting with RAD6. Thus, one RAD6 molecule can bind to the other R6BD and is positioned closely to another unoccupied RING domain for catalyzing the ligase function. Evidently, further experiments are required to elucidate this interesting possibility.

During the course of finally completing this manuscript, we have learned that Huang and co-workers have recently determined the structure of a RAD18 RING(1–99) dimer, also showing that this binds to RAD6 at a 2:2 ratio, whereas the full-length RAD18 dimer binds only to a single RAD6 molecule (54). Our study was conducted independently of their work.

SUPPLEMENTARY DATA

Supplementary Data are available at NAR Online: Supplementary Materials and Methods, Supplementary References [26,45,55].

ACKNOWLEDGEMENTS

The authors thank Dr Toshiki Tsurimoto (Kyushu University, Fukuoka, Japan) and Dr Tomohiko Ohta (St Marianna University School of Medicine, Kanagawa, Japan) for providing PCNA expression and ubiquitin-encoding plasmids, respectively. The authors would also like to express our appreciation to Dr Haruo Ohmori (Kyoto University, Kyoto, Japan) for his critical reading of manuscripts and valuable suggestions. The authors are grateful to Fumie Okubo, Kazumi Shimamoto and Mai Yoshida for their laboratory assistance.

FUNDING

Grants-in-Aid from the Ministry of Education, Culture, Sports, Science and Technology of Japan (to Y.M. and K.K.); Grants-in-Aid for Cancer Research from the Ministry of Health, Labour and Welfare (to K.K.). Funding for open access charge: Grants-in-Aid from the Ministry of Education, Culture, Sports, Science and Technology of Japan.

Conflict of interest statement. None declared.

REFERENCES

1. Deshaies,R.J. and Joazeiro,C.A. (2009) RING domain E3 ubiquitin ligases. *Annu. Rev. Biochem.*, **78**, 399–434.
2. Zheng,N., Wang,P., Jeffrey,P.D. and Pavletich,N.P. (2000) Structure of a c-Cbl-UbcH7 complex: RING domain function in ubiquitin-protein ligases. *Cell*, **102**, 533–539.

3. Brzovic,P.S., Rajagopal,P., Hoyt,D.W., King,M.C. and Klevit,R.E. (2001) Structure of a BRCA1-BARD1 heterodimeric RING-RING complex. *Nat. Struct. Biol.*, **8**, 833–837.
4. Hashizume,R., Fukuda,M., Maeda,I., Nishikawa,H., Oyake,D., Yabuki,Y., Ogata,H. and Ohta,T. (2001) The RING heterodimer BRCA1-BARD1 is a ubiquitin ligase inactivated by a breast cancer-derived mutation. *J. Biol. Chem.*, **276**, 14537–14540.
5. Xia,Y., Pao,G.M., Chen,H.W., Verma,I.M. and Hunter,T. (2003) Enhancement of BRCA1 E3 ubiquitin ligase activity through direct interaction with the BARD1 protein. *J. Biol. Chem.*, **278**, 5255–5263.
6. Buchwald,G., van der Stoop,P., Weichenrieder,O., Perrakis,A., van Lohuizen,M. and Sixma,T.K. (2006) Structure and E3-ligase activity of the Ring-Ring complex of polycomb proteins Bmi1 and Ring1b. *EMBO J.*, **25**, 2465–2474.
7. Satijn,D.P. and Otte,A.P. (1999) RING1 interacts with multiple Polycomb-group proteins and displays tumorigenic activity. *Mol. Cell. Biol.*, **19**, 57–68.
8. Kawai,H., Lopez-Pajares,V., Kim,M.M., Wiederschain,D. and Yuan,Z.M. (2007) RING domain-mediated interaction is a requirement for MDM2's E3 ligase activity. *Cancer Res.*, **67**, 6026–6030.
9. Linares,L.K., Hengstermann,A., Ciechanover,A., Muller,S. and Scheffner,M. (2003) HdmX stimulates Hdm2-mediated ubiquitination and degradation of p53. *Proc. Natl Acad. Sci. USA*, **100**, 12009–12014.
10. Linke,K., Mace,P.D., Smith,C.A., Vaux,D.L., Silke,J. and Day,C.L. (2008) Structure of the MDM2/MDMX RING domain heterodimer reveals dimerization is required for their ubiquitylation in trans. *Cell Death Differ.*, **15**, 841–848.
11. Mace,P.D., Linke,K., Feltham,R., Schumacher,F.R., Smith,C.A., Vaux,D.L., Silke,J. and Day,C.L. (2008) Structures of the cIAP2 RING domain reveal conformational changes associated with ubiquitin-conjugating enzyme (E2) recruitment. *J. Biol. Chem.*, **283**, 31633–31640.
12. Liew,C.W., Sun,H., Hunter,T. and Day,C.L. (2010) RING domain dimerization is essential for RNF4 function. *Biochem. J.*, **431**, 23–29.
13. Bailly,V., Lamb,J., Sung,P., Prakash,S. and Prakash,L. (1994) Specific complex formation between yeast RAD6 and RAD18 proteins: a potential mechanism for targeting RAD6 ubiquitin-conjugating activity to DNA damage sites. *Genes Dev.*, **8**, 811–820.
14. Bailly,V., Lauder,S., Prakash,S. and Prakash,L. (1997) Yeast DNA repair proteins Rad6 and Rad18 form a heterodimer that has ubiquitin conjugating, DNA binding, and ATP hydrolytic activities. *J. Biol. Chem.*, **272**, 23360–23365.
15. Notenboom,V., Hibbert,R.G., van Rossum-Fikkert,S.E., Olsen,J.V., Mann,M. and Sixma,T.K. (2007) Functional characterization of Rad18 domains for Rad6, ubiquitin, DNA binding and PCNA modification. *Nucleic Acids Res.*, **35**, 5819–5830.
16. Bailly,V., Prakash,S. and Prakash,L. (1997) Domains required for dimerization of yeast Rad6 ubiquitin-conjugating enzyme and Rad18 DNA binding protein. *Mol. Cell. Biol.*, **17**, 4536–4543.
17. Watanabe,K., Tateishi,S., Kawasuji,M., Tsurimoto,T., Inoue,H. and Yamaizumi,M. (2004) Rad18 guides polη to replication stalling sites through physical interaction and PCNA monoubiquitination. *EMBO J.*, **23**, 3886–3896.
18. Tateishi,S., Sakuraba,Y., Masuyama,S., Inoue,H. and Yamaizumi,M. (2000) Dysfunction of human Rad18 results in defective postreplication repair and hypersensitivity to multiple mutagens. *Proc. Natl Acad. Sci. USA*, **97**, 7927–7932.
19. Hibbert,R.G., Huang,A., Boelens,R. and Sixma,T.K. (2011) E3 ligase Rad18 promotes monoubiquitination rather than ubiquitin chain formation by E2 enzyme Rad6. *Proc. Natl Acad. Sci. USA*, **108**, 5590–5595.
20. Miyase,S., Tateishi,S., Watanabe,K., Tomita,K., Suzuki,K., Inoue,H. and Yamaizumi,M. (2005) Differential regulation of Rad18 through Rad6-dependent mono- and polyubiquitination. *J. Biol. Chem.*, **280**, 515–524.
21. Ulrich,H.D. and Jentsch,S. (2000) Two RING finger proteins mediate cooperation between ubiquitin-conjugating enzymes in DNA repair. *EMBO J.*, **19**, 3388–3397.
22. Friedberg,E.C., Walker,G.C., Siede,W., Wood,R.D., Schultz,R.A. and Ellenberger,T. (2006) DNA repair and mutagenesis. *2nd edn.* ASM, Washington, DC.
23. Hoege,C., Pfander,B., Moldovan,G.L., Pyrowolakis,G. and Jentsch,S. (2002) RAD6-dependent DNA repair is linked to modification of PCNA by ubiquitin and SUMO. *Nature*, **419**, 135–141.
24. Garg,P. and Burgers,P.M. (2005) Ubiquitinated proliferating cell nuclear antigen activates translesion DNA polymerases η and REV1. *Proc. Natl Acad. Sci. USA*, **102**, 18361–18366.
25. Haracska,L., Unk,I., Prakash,L. and Prakash,S. (2006) Ubiquitylation of yeast proliferating cell nuclear antigen and its implications for translesion DNA synthesis. *Proc. Natl Acad. Sci. USA*, **103**, 6477–6482.
26. Masuda,Y., Piao,J. and Kamiya,K. (2010) DNA replication-coupled PCNA mono-ubiquitination and polymerase switching in a human *in vitro* system. *J. Mol. Biol.*, **396**, 487–500.
27. Unk,I., Hajdu,I., Fatyol,K., Hurwitz,J., Yoon,J.H., Prakash,L., Prakash,S. and Haracska,L. (2008) Human HLTF functions as a ubiquitin ligase for proliferating cell nuclear antigen polyubiquitination. *Proc. Natl Acad. Sci. USA*, **105**, 3768–3773.
28. Unk,I., Hajdu,I., Fatyol,K., Szakal,B., Blastyak,A., Bermudez,V., Hurwitz,J., Prakash,L., Prakash,S. and Haracska,L. (2006) Human SHPRH is a ubiquitin ligase for Mms2-Ubc13-dependent polyubiquitylation of proliferating cell nuclear antigen. *Proc. Natl Acad. Sci. USA*, **103**, 18107–18112.
29. Bienko,M., Green,C.M., Crosetto,N., Rudolf,F., Zapart,G., Coull,B., Kannouche,P., Wider,G., Peter,M., Lehmann,A.R. *et al.* (2005) Ubiquitin-binding domains in Y-family polymerases regulate translesion synthesis. *Science*, **310**, 1821–1824.
30. Wood,A., Garg,P. and Burgers,P.M. (2007) A ubiquitin-binding motif in the translesion DNA polymerase Rev1 mediates its essential functional interaction with ubiquitinated proliferating cell nuclear antigen in response to DNA damage. *J. Biol. Chem.*, **282**, 20256–20263.
31. Zhuang,Z., Johnson,R.E., Haracska,L., Prakash,L., Prakash,S. and Benkovic,S.J. (2008) Regulation of polymerase exchange between Polη and Polδ by monoubiquitination of PCNA and the movement of DNA polymerase holoenzyme. *Proc. Natl Acad. Sci. USA*, **105**, 5361–5366.
32. Day,T.A., Palle,K., Barkley,L.R., Kakusho,N., Zou,Y., Tateishi,S., Verreault,A., Masai,H. and Vaziri,C. (2010) Phosphorylated Rad 18 directs DNA polymerase η to sites of stalled replication. *J. Cell. Biol.*, **191**, 953–966.
33. Bish,R.A. and Myers,M.P. (2007) Werner helicase-interacting protein 1 binds polyubiquitin via its zinc finger domain. *J. Biol. Chem.*, **282**, 23184–23193.
34. Crosetto,N., Bienko,M., Hibbert,R.G., Perica,T., Ambrogio,C., Kensche,T., Hofmann,K., Sixma,T.K. and Dikic,I. (2008) Human Wrnip1 is localized in replication factories in a ubiquitin-binding zinc finger-dependent manner. *J. Biol. Chem.*, **283**, 35173–35185.
35. Hofmann,K. (2009) Ubiquitin-binding domains and their role in the DNA damage response. *DNA Repair*, **8**, 544–556.
36. Aravind,L. and Koonin,E.V. (2000) SAP - a putative DNA-binding motif involved in chromosomal organization. *Trends Biochem. Sci.*, **25**, 112–114.
37. Nakajima,S., Lan,L., Kanno,S., Usami,N., Kobayashi,K., Mori,M., Shiomi,T. and Yasui,A. (2006) Replication-dependent and -independent responses of RAD18 to DNA damage in human cells. *J. Biol. Chem.*, **281**, 34687–34695.
38. Tsuji,Y., Watanabe,K., Araki,K., Shinohara,M., Yamagata,Y., Tsurimoto,T., Hanaoka,F., Yamamura,K., Yamaizumi,M. and Tateishi,S. (2008) Recognition of forked and single-stranded DNA structures by human RAD18 complexed with RAD6B protein triggers its recruitment to stalled replication forks. *Genes Cells*, **13**, 343–354.
39. Huang,J., Huen,M.S., Kim,H., Leung,C.C., Glover,J.N., Yu,X. and Chen,J. (2009) RAD18 transmits DNA damage signalling to elicit homologous recombination repair. *Nat. Cell. Biol.*, **11**, 592–603.
40. Fukuda,K., Morioka,H., Imajou,S., Ikeda,S., Ohtsuka,E. and Tsurimoto,T. (1995) Structure-function relationship of the eukaryotic DNA replication factor, proliferating cell nuclear antigen. *J. Biol. Chem.*, **270**, 22527–22534.